Bioactive Materials 33 (2024) 424–443

Contents lists available at ScienceDirect

Bioactive Materials

journal homepage: www.keaipublishing.com/en/journals/bioactive-materials

Local delivery of EGFR$^+$NSCs-derived exosomes promotes neural regeneration post spinal cord injury via miR-34a-5p/HDAC6 pathway

Tian Qin [a,b,c,1], Chengjun Li [b,c,d,1], Yan Xu [b,c,d], Yiming Qin [a,b,c], Yuxin Jin [a,b,c], Rundong He [a,b,c], Zixiang Luo [a,b,c], Jinyun Zhao [a,b,c], Chunyue Duan [a,b,c], Hongbin Lu [b,c,d,***], Yong Cao [a,b,c,*], Jianzhong Hu [a,b,c,**]

[a] Department of Spine Surgery and Orthopaedics, Xiangya Hospital, Central South University, Xiangya Road 87, Changsha, 410008, China
[b] Key Laboratory of Organ Injury, Aging and Regenerative Medicine of Hunan Province, Xiangya Road 87, Changsha, 410008, China
[c] National Clinical Research Center for Geriatric Disorders, Xiangya Hospital, Central South University, Xiangya Road 87, Changsha, 410008, China
[d] Department of Sports Medicine, Xiangya Hospital, Central South University, Xiangya Road 87, Changsha, 410008, China

ARTICLE INFO

Keywords:
Spinal cord injury
Exosomes
Neural regeneration
miR-34a-5p
HDAC6

ABSTRACT

Spinal cord injury (SCI) causes severe axon damage, usually leading to permanent paraparesis, which still lacks effective regenerative therapy. Recent studies have suggested that exosomes derived from neural stem cells (NSCs) may hold promise as attractive candidates for SCI treatment. Epidermal Growth Factor Receptor positive NSC (EGFR$^+$NSC) is a subpopulation of endogenous NSCs, showing strong regenerative capability in central nervous system disease. In the current study, we isolated exosomes from the EGFR$^+$NSCs (EGFR$^+$NSCs-Exos) and discovered that local delivery of EGFR$^+$NSCs-Exos can effectively promote neurite regrowth in the injury site of spinal cord-injured mice and improve their neurological function recovery. Using the miRNA-seq, we firstly characterized the microRNAs (miRNAs) cargo of EGFR$^+$NSCs-Exos and identified miR-34a-5p which was highly enriched in EGFR$^+$NSCs derived exosomes. We further interpreted that exosomal miR-34a-5p could be transferred to neurons and inhibit the HDAC6 expression by directly binding to its mRNA, contributing to microtubule stabilization and autophagy induction for aiding SCI repair. Overall, our research demonstrated a novel therapeutic approach to improving neurological functional recovery by using exosomes secreted from a subpopulation of endogenous NSCs and providing a precise cell-free treatment strategy for SCI repair.

1. Materials and methods

1.1. Bioinformatic analysis of the single-cell transcriptomic dataset

The single-cell RNA sequencing data of the neural stem cells from the mice subventricular zone (SVZ) samples was retrieved from the GEO database (GSE67833). CellRanger (v6.1.2) software was used to transform the Illumina output into gene-barcode count matrices for further analysis in our study. Data processing and analysis were performed using the R package "Seurat" (v5.0). Cells having >6000 genes and >20 % of mitochondrial transcripts were removed. The gene expression matrix was normalized and scaled. We selected the top 50 principal components by performing Principal Component Analysis (PCA) based on 5000 variable genes. The "harmony" algorithm was applied to correct the batch effect. The FindNeighbors and FindClusters functions were used to cluster cells on a shared-nearest-neighbor graph. Clusters were annotated to each cell type based on markers from the previous study. A uniform Manifold Approximation and Projection (UMAP) plot was used to visualize annotated cell clusters. The markers of each cell type were calculated using the FindAllMarkers function, which compares gene expression between clusters by performing the Wilcoxon rank-sum test. While analyzing the NSCs clusters, 2 main clusters were identified.

Peer review under responsibility of KeAi Communications Co., Ltd.
* Corresponding author. Department of Spine Surgery and Orthopedics, Xiangya Hospital, Central South University, Xiangya Road 87, Changsha, 410008, China.
** Corresponding author. Department of Spine Surgery and Orthopaedics, Xiangya Hospital, Central South University, Xiangya Road 87, Changsha, 410008, China.
*** Corresponding author. Department of Sports Medicine, Xiangya Hospital, Central South University, Xiangya Road 87, Changsha, 410008, China.
E-mail addresses: hongbinlu@csu.edu.cn, hongbinlu@hotmail.com (H. Lu), xycaoyong@csu.edu.cn, caoyong1912@163.com (Y. Cao), jianzhonghu@csu.edu.cn, jianzhonghu@hotmail.com (J. Hu).
[1] These authors contributed equally.

https://doi.org/10.1016/j.bioactmat.2023.11.013
Received 2 August 2023; Received in revised form 18 November 2023; Accepted 19 November 2023

Among them, the cluster with relatively high expression of EGFR was defined as the aNSCs. The GO, KEGG pathway enrichment and GSEA of the marker genes were performed as above.

1.2. Animal ethical statement

Animals were maintained in standard, specific pathogen-free conditions of the Department of Laboratory Animals, Central South University (CSU) with 12 light/12 dark cycles and 4–5 mice per cage. All mice in this study were kept on a standard normal chow diet. All animal experiments were approved by the Ethics Committee of CSU for Scientific Research.

1.3. Cell culture

The primary culture of NSC was performed as described previously [1,2]. Briefly, the cortex and spine were dissected from the E14C57BL/6 mice, cut into small pieces (~1 mm3), and followed by digestion via Accutase™ (Invitrogen, United States) for 30 min at 37 °C. After centrifugation, cells were suspended in an NSC medium composed of Neurobasal-A (Gibco, United States), 0.24 % GlutaMAX™ Supplement (Gibco, United States), 2 % B27 without vitamin A (Gibco, United States), 10 ng/mL EGF (Sigma, United States), 10 ng/mL bFGF (Sigma, United States) and 1 % penicillin-streptomycin and seeded in ultralow adhesion 6-well plates (Corning, United States), and 3 days later, neurospheres were collected via centrifugation and digested through Accutase into single cells, passed and maintained in neurosphere culture media until experimental use.

Primary cortical neurons were extracted from the cerebral cortices of fetal C57BL/6 mice and washed twice with phosphate buffer saline (PBS). After removal of the dura mater, the cortex was separated in Dulbecco's modified Eagle's medium (DMEM, HyClone, United States) and pipetted with a Pasteur pipetted for homogenization. After centrifugation at 1000 rpm, the cells were resuspended and cultured with neurobasal medium containing 2 % B27, 1 % glutamine (Gibco, United States), and 1 % penicillin-streptomycin in a poly-lysine pre-coated plate [3,4]. HEK293T cells were purchased from Procell (Gibco, United States) and were cultured in Dulbecco modified Eagle medium (DMEM) containing 10 % fetal bovine serum and 1 % penicillin-streptomycin.

1.4. Microfluidic culture assay

The SND450 culture plate was used to detect the axon extension [5]. The compartments for axon and soma are separated by a physical partition that has a number of embedded micrometer-sized grooves. The axons generated from neurons plated into the soma compartment could extend across the barrier through the microgrooves. Briefly, the primary isolated neurons were seeded on the somal compartment. After culturing for 7 days, the axons crossing the 450 μm-microtunel were cut off using a 200 μL pipette. 24 h later, the regenerative axons were stained and the total regenerative axonal length was calculated.

1.5. Flow cytometry and cell sorting

The cortex tissues were dissected from 14 d-embryonic C57BL/6 mice after removing surrounding meninges. The cell sorting process was administrated as previous reported [6]. Briefly, the remained tissues were pipetted until tissue pieces were dissociated into single cells in Hanks balanced alt Solution (Life Technologies, United States) containing 10 mM HEPES (Gibco, United States). After washing, the anti-mouse CD16/CD32 antibody (Fc Receptor Blocking Solution) (BD, United States) was added to the single cell suspension according to a 1/50 dilution ratio, incubating at 4 °C for 15 min. Next, the harvest cells were resuspended in a staining buffer and stained with antibodies for 30 min at 4 °C. The antibodies were as follows: Anti-CD133-APC (Thermal, United States), Anti-Glast-PE (Miltenyi, Germany), EGF-Alexa 647 (Thermal, United States), Anti-CD45-Alexa700 (Thermal, United States), Anti-Ter 119-PE/Cy7 (Thermal, United States). After washing, cells were resuspended in PBS with 2 mM EDTA (Thermal, United States). and 1 μg/mL 4–6, Diamidino-2-Phenylindole (DAPI, BD, United States). The sample was sorted using a FACS Aria II SORP cell sorter (BD Biosciences) cytometer, and then analyzed utilizing FlowJo software (TreeStar). $DAPI^+$ cells and doublets were excluded during the analysis.

To knockdown miR-34a-5p in exosomes and verify its function, we transfected isolated $EGFR^+$NSCs with a miR-34a-5p inhibitor or a negative control (NC) (Hanbio, China) at a concentration of 100 nM using Lipofectamine 3000 (Hanbio, China). The sequences for the miR-34a-5p inhibitor and negative control (NC) were listed as follows: miR-34a-5p inhibitor (5′-ACAACCAGCUAAGACACUGCCA-3′) and miR-34a-5p NC (5′-UCACAACCUCCUAGAAAGAGUAGA-3′).

1.6. Isolation and identification of exosomes

Exosomes were isolated from the primary and $EGFR^+$NSCs supernatant by differential centrifugation/ultracentrifugation protocols [7]. In our experiment, after first passage and 3 days of continuous culture, the cell supernatant was collected from the primary and $EGFR^+$NSCs. The obtained medium was centrifuged at 300 g for 15 min and 2,000 g for 30 min to remove the remaining debris. The resulting solution was further processed by centrifugation at 10,000 g for 1 h to remove any remaining cellular debris. The supernatant was then subjected to ultracentrifugation at 100,000 g for 2 h to obtain the exosomal pellet, which was subsequently resuspended in PBS. This suspension was then subjected to another ultracentrifugation at 100,000 g for 2 h. Finally, the pelleted exosomes were resuspended in PBS. The morphology of the exosomes was characterized by transmission electron microscopy (TEM) using fresh samples that were loaded onto a continuous carbon grid, fixed in 3 % (w/v) glutaraldehyde, and stained with 2 % uranyl acetate. The size and concentration of the exosomes were assessed using flow NanoAnalyzer instruments, following the manufacturer's instructions. The presence of exosomal markers CD9, TSG101, and CD63 and the cell marker Calnexin were detected by immunoblotting analysis.

1.7. Preparation and characterization of the hydrogel

The hydrogel was synthesized according to the previously reported protocol [8]. Briefly, the 10 % (w/v) Gelatin methacryloyl (GelMA) and 2.5 % (w/v) N-(2-aminoethyl)-4-(4-(hydroxymethyl)-2-methoxy -5-nitrosophenoxy butanamide linked to the glycosaminoglycan hyaluronic acid (HA-NB) were prepared in advance. Then the 10 % GelMA, 2.5 % HA-NB and the polymerization initiator lithium phenyl-2,4, 6-trimethylbenzoylphosphinate (LAP) were mixed to a final concentration of 3.75 % (w/v) GelMA, 0.94 % (w/v) HA-NB and 0.1 % (w/v) LAP. The microstructure of hydrogels was characterized by scanning electron microscope (SEM). The photocured hydrogel was fixed in 2.5 % glutaraldehyde for 90 min, dehydrated with a graded ethanol series, then freeze-dried for 2 days. Dried samples were coated with gold and examined via SEM. We evaluated the in vitro degradation of the hydrogels by creating 100 μL GelMA hydrogels, initially weighing them as Md0. Subsequently, these hydrogels were immersed in a pH 7.4 PBS solution and placed in a shaker at 4 °C for 28 days. At specific intervals (0, 1, 3, 7, 10, 14, 21, and 28 days), we absorbed the supernatant and recorded the hydrogel's weight as Mdt. The degradation rate of the hydrogels was determined using the formula DR=((Mdt-Md0)/Md0) *100 % [9]. Hydrogel samples (100 μL) were photopolymerized in a 1.5 mL tube and 1 mL PBS was gently added. Samples were incubated at 37 °C. At each time point (0, 3 h, 6 h, 12 h, 24 h, 3 d, 5 d, and 7 d), the PBS was removed and the swollen weight of the hydrogel sample was recorded (Wwet). Samples were then frozen at −80 °C, lyophilized, and the dry weight (Wdry) was recorded. The swelling ratio was calculated as Wwet/Wdry [10].

1.8. Exosomes loading and sustained releasing test in vitro

To load exosomes, we introduced the exosome suspension into the hydrogel solution, resulting in a final concentration of 10 mg/mL. Afterward, we bio-fabricated a 3D-printed hydrogel patch using dynamic projection stereolithography based on the shape of the removed lamina [11]. This hydrogel containing PKH67 labeled exosomes was then utilized for confocal imaging (LSM780, Zessis) with multilayer scanning and subsequent 3D reconstruction.

To generate the release profile for primary and $EGFR^{+}$NSCs-Exos loaded hydrogel, we immersed 100 μL of exosomes-loaded hydrogel (10 mg/mL, post UV irradiation) in 500 μL of PBS dissolution medium at 37 °C. At regular intervals, we replenished the same volume of pre-heated PBS dissolution medium after collecting 500 μL of the sample. To quantitatively determine exosome release, we employed the Micro BCA™ Protein Assay Kit (ThermoFisher, Rockford, USA) [12]. The release profile was constructed based on the release data.

1.9. Exosome fluorescent label and uptake assay both in vitro and in vivo

Exosomes were labeled with DiR and PKH67 (Sigma, United States) according to the manufacturer's protocol. In Brief, 4 μL dye was mixed with exosome suspension in diluent C and incubated for 10 min at 37 °C. The labeling reaction was stopped by adding 20 mL of chilled PBS. Labeled exosomes were then ultracentrifuged at 100,000 g for 70 min, washed with PBS, ultracentrifuged again at 100,000 g and the pellet was resuspended in PBS. For the in vitro uptake experiment, PKH67 labeled neural stem cell exosomes were added to the neuron cell culture medium (10 μg/mL) and incubated for 12 h at 37 °C and 5 % CO_2. After the set time, the neuron-related marker Tuj1 was immunofluorescently stained to label the cultured neurons. For in vivo tracking of neural stem cell exosomes, a mixture of DiR or PKH67 fluorescent-labeled exosomes and a photosensitized-hydrogel patch was placed above the lesion of spinal cord injury. Three days post-injury, the spinal cord tissue was harvested and sectioned for immunostaining to analyze the uptake of exosomes by injured and peripheral neurons. The mice treated with DiR-labeled exosomes were anesthetized at 1, 3, 7, 14, and 28 days post-SCI transplantation and placed in a Xenogen IVIS Imaging System (Caliper Life Sciences).

1.10. Exosomal miRNA microarray assay

Total RNA was extracted from exosomes using TRIzol reagent (Invitrogen, United States) following the manufacturer's instructions. The quality of the RNA samples was evaluated using the NanoDrop ND-1000 and Agilent 2100 Bioanalyzer. After passing the quality check, a small RNA sample pre-kit was used to construct the library. The library was constructed by directly splicing the two ends of small RNA, starting from total RNA as the sample, using the special structure of the 3′ and 5′ ends of small RNA (complete phosphate group at the 5′ end and hydroxyl group at the 3′ end). The cDNA was synthesized by reverse transcription after the splicing, followed by Polymerase Chain Reaction (PCR) amplification to obtain the target DNA fragments. The cDNA library was obtained by cutting the gel and recycling it. The quality and quantity of the library were checked carefully using automated electrophoresis on an Agilent 2100 Bioanalyzer. The different libraries were pooled based on the effective concentration and target offline data volume, followed by Hiseq/Miseq sequencing.

1.11. Fluorescent miRNA in situ hybridization

Biotin-labeled miR-34a-5p (Sangon Biotech, China) was constructed for fluorescent miRNA in situ hybridization as previously described [13]. Briefly, the paraffin-embedded tissues were cut into 8 μm thick sections. After dewaxed with xylene and rehydrated in an ethanol gradient, the proteinase K (20 μg/mL, Ambion) was administrated to the sections for 30min. After washing with PBS, the sections were incubated with the hybridization buffer at 37 °C for 1 h for prehybridization. Next, the sections were incubated with the hybridization buffer containing miR-34a-5p-biotin probe (sequence: 5′-biotin- ACAACCAGCUAAGACACUGCCA-biotin-3′) at 60 °C for 8 h. After incubation, the slices were sequentially washed with 2 × SSC, 1 × SSC, and 0.5 × SSC buffer. The Anti-Neun antibody was administered to stain the spinal neurons, and the 4′,6-diamidino-2-phenylindole (DAPI) solution was used to stain the nucleus. The region of interest (ROI) was selected from the anterior horn of the spinal cord at 500 μm rostrally adjacent to the injured site in the horizontal spinal cord sections. For quantification, the relative immunofluorescent intensity ratio of miR-34a-5p in the NeuN positive area was measured by ImageJ software (National Institutes of Health, USA).

1.12. In vitro neurite outgrowth assay

Primary neurons were isolated from 14-day embryos of C57/BL6 mice and culture as previously described. These neurons were then cultured with primary NSCs-Exos and $EGFR^{+}$NSCs-Exos to investigate their ability to promote neurite outgrowth. To test functional recovery, HDAC6 overexpress plasmids and their corresponding control vectors were transfected into primary cultured neurons before treatment with exosomes. At least 5 random fields per group were measured, and all measurements were performed by experimenters blinded to each treatment condition. A neurite outgrowth assay was carried out on cortical neuron cells under various treatment conditions using β–III–tubulin (Tuj1) immunofluorescence staining. DAPI counterstaining was done to visualize neuron cell nuclei. Fluorescent red images (showing cell body and neurites) were merged with fluorescent blue images (showing cell nuclei) to analyze a complete image. Tuj1 positive cells and nuclei with blue fluorescent signals from stained neurons were quantified using the ImageJ software and digitized with an immunofluorescence microscope (Zeiss, Germany).

1.13. Histology and immunofluorescence analysis

The spinal cords and bladders of mice were harvested after perfused with 4 % paraformaldehyde. Following gradient alcohol dehydration, the spinal cords and bladders were embedded in paraffin, horizontally sectioned at a thickness of approximately 8 μm, and subjected to H & E staining as per the instructions of the H & E staining kit (Solarbio, China). Images were captured using an Olympus photomicroscope. To define "the injury area", the normal tissue replaced by vacuoles and gliomatoid tissues was outlined. The injury area of the spinal cord and the thickness of the bladder's muscular layer were manually outlined and calculated using ImageJ. For immunohistochemistry analysis, after dehydration, the paraffin spinal sections were stained using an immunohistochemical kit (Yeason, China). The antibody dilution concentration is as follows: anti-HDAC6 (1:500, sigma), anti-Acetylated α-tubulin (1:100, sigma), anti-LC3 (1:100, proteintech). For Immunofluorescence analysis, the spinal cord slices were immersed in PBS buffer for 15 min to remove the O·C.T compound. They were then permeabilized with 0.1 % Triton X-100 in PBS buffer for 15 min to break the membrane and blocked with 5 % bovine serum albumin (BSA) for 30 min. The cell samples were fixed with 4 % Paraformaldehyde (PFA) in PBS for 20 min, permeabilized with 0.1 % Triton X-100 for 15 min, and blocked with 5 % BSA for 30 min. The diluted antibodies anti-GAP43 (1:200, CST), anti-NF (1:200, CST), anti-NeuN (1:500, Abcam), anti-HDAC6 (1:500, proteintech), anti-Acetylated α-tubulin (1:500, sigma), anti-Tyrosinated α-tubulin (1:500, sigma), anti-LC3 (1:500, proteintech) anti-Nestin (1:500, Abcam), and anti-SOX2 (1:500, Abcam), were then added and incubated with the samples for 8–10 h at 4 °C. After rinsing the slices with PBS, the samples were incubated with the respective diluted fluorescent secondary antibody (1:500; Abcam) for 1.5 h at room temperature. Finally, a DAPI (GeneTex, United States) solution containing a sealing agent was

added dropwise to stain the nucleus. The Region of interest (ROI) of HDAC6, miR-34a-5p, and Acetylated α-tubulin/Tyrosinated α-tubulin was selected from the anterior horn of the spinal cord at 500 μm rostrally adjacent to the injured epicenter. Images were captured by an Axio Imager one microscope (Zeiss, Germany).

1.14. Establishment of contusive spinal cord injury mouse model and experimental design

All of the mice were anesthetized with 0.3 % pentobarbital sodium before undergoing thoracic spinal cord contusion injuries. A moderate contusion injury was induced by using a modified Allen's weight drop apparatus, dropping a 10 g weight at a vertical height of 25 mm after laminectomy at T10 [13]. Mice in the sham group underwent laminectomy without contusion. Bladders were manually massaged twice daily until full voluntary or autonomic voiding was achieved. The animals were randomly divided into different intervention groups (N = 5) according to the study design, to analyze the effect of exosomes on spinal cord injury functional recovery. The sham group was subjected to laminectomy without spinal cord injury. Mice in the experimental group were administered with solid hydrogel patches containing exosomes (10 mg/mL) or SW-100 (10 mg/mL) based on the grouping assignment upon the injury site. The vehicle group was given an equal size of hydrogel mix with an equal volume of PBS. At the scheduled time point post-SCI, mice were euthanized, and the spinal cord tissue containing the lesion site was collected and processed for analysis described in the method.

1.15. Behavioral functional evaluations

BMS (Basso mouse scale) score was scored independently by 2 observers who were blinded to the experimental group information. The assessments were made before the injury, immediately after the injury, and on day 1, day 3, day 7, day 14, day 21, and day 28 post-injury [14]. Specifically, the study involved placing mice in an open field for 4 min to evaluate the motor recovery capabilities of mice with spinal cord injuries. The evaluation was based on a scoring system that ranged between 0 and 9. This system was determined by hind limb movement in the open field, such as joint movement in the hind limb, weight support, foot stepping, coordination, claw positioning, and trunk and tail control. A score of 0 indicated complete hind limb paralysis, while a score of 9 indicated normal movement.

1.16. MEPs recording

The mice were anesthetized using 0.3 % Pentobarbital Sodium. They were shaved and disinfected before being secured in the stereotactic apparatus, and their body temperature was maintained with a heating pad. The motor cortex area was exposed by craniotomy, and the stimulation electrode was guided to a depth of 700–1000 μm from the brain surface using a stereotactic instrument. The target was the corticospinal neurons in the sensorimotor cortex. The recording electrode was positioned at the distal end of the contralateral thigh sciatic nerve to capture the muscle action potential triggered by electrical stimulation. The Bl-420 F biological function experimental system was utilized to amplify and record the bioelectrical signal. The stimulation parameters included fine voltage stimulation, single stimulation mode, 100 ms delay, and 100 Hz frequency, with a stimulation intensity of 14 V [3].

1.17. Quantitative RT-qPCR

Total RNA was extracted from exosomes and cultured neurons (3 days post-transfection or exosomal treatment) using TRIzol reagent (Invitrogen, United States). The cDNA was then reverse transcribed using the PrimeScript™ RT Reagent kit (Promega, United States) according to the manufacturer's instructions. Additionally, the reverse transcription of miRNAs was performed using the miRNA First Strand cDNA Synthesis kit (Tailing Reaction, Sangon Biotech, China). The pri-miRNAs were synthesized into the cDNA using the miRNA 1st Strand cDNA Synthesis Kit (by stem-loop, Sangon Biotech, China). For the measurement of mRNAs and miRNAs, qRT-PCR was carried out using a GoTaq qPCR Master Mix kit (Promega, United States), as well as a quantitative PCR system (ABI, United States). To evaluate the relative expression levels of mRNA or miRNA, the $2^{-\Delta\Delta CT}$ method was employed with *GAPDH* and *U6* serving as internal references. The primers that were used for qRT-PCR can be found in Table S1.

1.18. Luciferase reporter assay

HDAC6 plasmid, mimics of miR-34a-5p, and miR-34a-5p negative control (NC) were constructed by Hanbio Biology (China, Shanghai). The wild-type HDAC6 containing miR-34a-5p binding site and the binding sequence of 3′UTR and mutation were cloned into a psi-check 2 plasmid, which was called HDAC6-WT and HDAC6-MUT respectively. The renal epithelial cell lines (293 T cells) were co-transfected with luciferase reporter gene constructs (HDAC6-WT or HDAC6-MUT) and miRNAs (NC or miR-34a-5p). Two days after transfection, the double luciferase reporter gene detection kit was used to detect the fluorescence intensity ratio of 293 T cells in each group. The sequence of miR-34a-5p is 5′UGGCAGUGUUAGCUGGUUGU3'; the sequence of miR-34a-5p –NC is 5′UCACAACCUCCUGAAAGAGUAGA3' [15].

1.19. Autophagy detection

According to the manufacturer's instructions, the primary cortical neurons that had been previously separated were planted on confocal dishes and subsequently transfected with the mRFP-GFP-LC3 adenovirus (Hanbio Biology, China) [16]. After transfection, cells were fixed in 4 % paraformaldehyde and photographed using a laser confocal microscope (Zeiss, Germany). The quantity of red and yellow dots, corresponding to autolysosomes and autophagosomes, respectively, was measured. For transmission electron microscope (TEM) assessment, the cell pellet was fixed with a 2 % glutaraldehyde solution, pre-cooled, and then stained with a 2 % uranyl acetate solution. The cells were finally dehydrated in acetone, embedded, and cut into thin slices for examination under an electron microscope (FEI Tecnai, Hillsboro, OR, USA).

1.20. Western blotting

Total protein was isolated from exosomes, and cultured neurons (3 days post exosomal treatment or transfection) using RIPA lysis buffer (Beyotime, China) following the manufacturer's protocol. The protein concentration was measured using a BCA kit (Multisciences, China). Equal amounts of protein samples were separated by 10 % sodium dodecyl sulfate-polyacrylamide gel electrophoresis and transferred onto a polyvinylidene fluoride (PVDF) membrane. The transferred PVDF film was then immersed in 5 % fat-free milk at room temperature for 2 h. After blocking, the membranes were incubated overnight at 4 °C with primary antibodies against β-Actin (1:5000, Abcam), CD63 (1:1000, Abcam), TSG101 (1:1000, Abcam), CD9 (1:1000, Abcam), calnexin (1:1000, Abcam), acetylated α-tubulin (1:1000, Abcam), and tyrosinated α-tubulin (1:1000, Abcam). Following the incubation, the PVDF membrane was washed with Tris-buffered saline with 0.1 % Tween® 20 Detergent (TBST)thrice and then incubated with HRP-labeled secondary antibody at room temperature for 90 min, followed by three washes with TBST buffer for 10 min each time. Enhanced chemiluminescence reagent was used to visualize immunoreactive bands.

1.21. Statistical analysis

Results are represented as mean values ± SD, and n values represent the number of animals in the experiments. Statistical analysis was carried out using Prism 8 software. Differences were considered statistically

significant at values listed as follows: $^{*}P < 0.05$, $^{**}P < 0.01$, and $^{***}P < 0.001$. Statistical comparisons of two groups were conducted using a two-tailed unpaired Student's t-test. Differences among multiple groups were analyzed with one-way ANOVA followed by Tukey's post hoc tests. The analysis of BMS scores and tactile sensory tests were analyzed with repeated-measures two-way ANOVA at different time points.

2. Introduction

Spinal cord injury (SCI) is a devastating event that results in neurologic deficits such as motor, sensory, and autonomic (sexual, urinary, and gastrointestinal) dysfunction [17]. SCI has a high prevalence globally, affecting an estimated 40–80 per million people every year [18,19]. Long-term disability places huge financial, physical, and psychological burdens on both their families and society [20]. Although the treatment of spinal cord injury has made significant progress in the laboratory [21], there is currently no effective clinical treatment that can improve the poor prognosis after SCI.

The adult mammalian central nervous system (CNS) is considered an organ with limited regeneration capability [22,23]. However, the discovery of endogenous NSCs in specific niches of the adult brain and spinal cord provides evidence that CNS may be generative by inducing the differentiation of endogenous NSCs into neurons [24–26]. There are also endogenous neural precursor cells in the spinal cord tissue of adult mice, called Ependyma cells. While, compared with NSCs in brain, most ependymal cells located in the central canal of the spinal cord tend to differentiate into astrocytes rather than mature neurons after SCI [23]. Exogenous NSCs-based therapy may be a feasible option to promote function recovery after SCI. In a phase I clinical trial, human spinal cord-derived NSCs were found to have good histocompatibility and could be safely transplanted into damaged spinal cord in patients with thoracic SCI [27]. The favorable effects of NSC grafts have been demonstrated due to their unique neuroprotective effects, including affecting axon plasticity, regeneration, sprouting, and establishment of neuronal relays at the injury site [28–30]. However, there are also some concerns that direct transplantation of NSCs may have deleterious effects such as cell necrosis, immune rejection, and even tumor formation, which may limit their application in SCI treatment [31,32].

Exosomes are a form of extracellular vesicles with a diameter of 30–150 nm, serving as a medium for intercellular communication [33]. Due to their low immunogenicity, exosomes are increasingly being used as a potential cell-free therapy for CNS injury healing [34,35]. Adult NSCs can be divided into two states: static state (outside the cell cycle, in a low metabolic state) and active state (inside the cell cycle), which is mainly located in SVZ region. The quiescent state of NSCs is closely related to astrocytes, and the active state of NSCs shows an obvious tendency to neurogenesis [36]. In craniocerebral injury, the activation of active NSCs ($CD133^{+}EGFR^{+}$) increased and repaired the damaged area, suggesting that active NSCs play an important role in the repair of nerve injury [25]. However, whether these active NSCs, as a subset of stem cells with potential neurogenesis, could play a role in the treatment of SCI remains to be studied.

In a mouse model following thromboembolic stroke, intravenous treatment of NSCs-derived extracellular vehicles (EVs) improved functional outcomes [37]. Rong et al. also found in a rat model that NSCs-derived EVs could promote functional recovery after SCI by activating autophagy [38,39]. Our previous study also showed that exosomes produced by NSCs improved functional recovery after SCI by promoting angiogenesis [2]. However, it is unclear whether exosomes produced by $EGFR^{+}$NSCs, a subtype of NSCs, are comparable or stronger than primary NSCs-derived exosomes in terms of neurological recovery after SCI. Exosomes alter the biological activity of target cells by transferring messenger RNAs, miRNAs, lipids, and proteins [33]. MicroRNAs (miRNAs) are components of exosomal cargo and play a key role in mediating the therapeutic effects in various neurodegenerative diseases [40]. Through high-throughput sequencing, we found that $EGFR^{+}$NSCs-derived exosomes were enriched in miR-34a-5p. However, whether exosomes affect neurite growth and functional repair through miRNAs still needs to be further explored.

However, the stability and retention of exosomes released in vivo are major barriers, as they are rapidly eliminated by the innate immune system or accumulate in the liver and lungs via body fluids or blood circulation [44]. Various biomaterials have been employed to create tissue engineering scaffolds for spinal cord injury (SCI), including natural materials such as hyaluronic acid (HA), collagen-based matrices, chitosan, agarose, alginate, etc [41–43]. Loading exosomes in a protective hydrogel, which is a hydrophilic polymer network, may shield them from degradation and offer a prolonged reservoir for therapeutic actions [45]. Thus, in the current study, exosome-loaded hydrogels were used to print into patches based on the shape of removed lamina using 3D printing technology and placed cover the injury lesion of the spinal cord, and we found that exosomes secreted by $EGFR^{+}$NSCs showed a more powerful therapeutic effect on functional recovery of SCI than primary NSC derived exosomes. The $EGFR^{+}$NSCs derived exosomes could deliver miR-34a-5p to neurons to downregulate histone deacetylase 6 (HDAC6), which in turn activated autophagy process and enhanced neurite growth. Our study proposed a new type of exosomes derived from $EGFR^{+}$NSCs with the potential capability to improve functional recovery after SCI, which provided a new cell-free therapy for the treatment of SCI (Fig. 1).

3. Results

3.1. Identification of primary and EGFR-positive NSCs and their secreted extracellular vesicles

First, we projected the $GLAST^{+}CD133^{+}$ cells onto a Uniform Manifold Approximation and Projection (UMAP) to visualize clustering according to the published data (GSE67833) (Fig. 2A). The NSCs were clustered into aNSCs and qNSCs, the aNSCs showed high expression of *Egfr* a known marker of active NSCs (Fig. 2B–C). To obtain functional insights into the gene classes that define each cell subtype, we performed gene ontology on the four clusters. From this, we determined the aNSCs expressed genes highly enriched in GO biological process pathways related to neural development and reparation (Microtubule organizing center localization, Negative regulation of neuron death, Negative regulation of oxidative stress−induced neuron death, Positive regulation of neuron projection development) (Fig. 2D–E). To explore the therapeutic effects of the aNSCs in SCI treatment, using flow cytometry, the living $EGFR^{+}$ neural stem cells ($EGFR^{+}$NSCs) were sorted by the panel of $DAPI^{-}$(living cell), $CD45^{-}$ and Ter 119^{-} (none blood cells) and $GLAST^{+}CD133^{+}EGFR^{+}$(active NSCs) in the subventricular zone from E14 fetal mice cerebral cortex (Fig. 2F). About 2.159 ± 0.315 % of cells from the fetal mice cortex brain were GLAST, CD133 and EGFR triple positive. The stem cell markers Nestin and Sox2 were expressed in the sorted $EGFR^{+}$NSCs (Fig. 2G). To verify whether all cells expressing EGFR, we passed $EGFR^{+}$NSCs into P1, P2, and P3 and detected EGFR expression in NSCs by flow cytometry and immunofluorescent staining. We found that the EGFR positive rate of NSC still reached up to 90 % even after three passes, indicating that the cell phenotype we extracted did not change over time (Fig. 2H–I). Then the exosomes were extracted from primary NSCs and $EGFR^{+}$NSCs culture media. According to high-resolution transmission electron micrographs (TEM) images, exosomes released by primary NSCs (primary NSCs-Exos) and $EGFR^{+}$NSC ($EGFR^{+}$NSCs-Exos) exhibit characteristic rounded and cup-like architectures (Fig. 2J). Primary NSCs-Exos and $EGFR^{+}$NSCs-Exos have a homogenous size distribution with an average single peak at 75.21 nm and 74.2 nm, which was revealed by nanoparticle tracking analysis (Fig. 2K). Western blotting showed that both Primary NSCs-Exos and $EGFR^{+}$NSCs-Exos express the exosomal surface markers CD63, CD9, and TSG101 without negative biomarkers of calnexin (Fig. 2L), revealing that the separated particles were exosomes released from primary or $EGFR^{+}$NSCs.

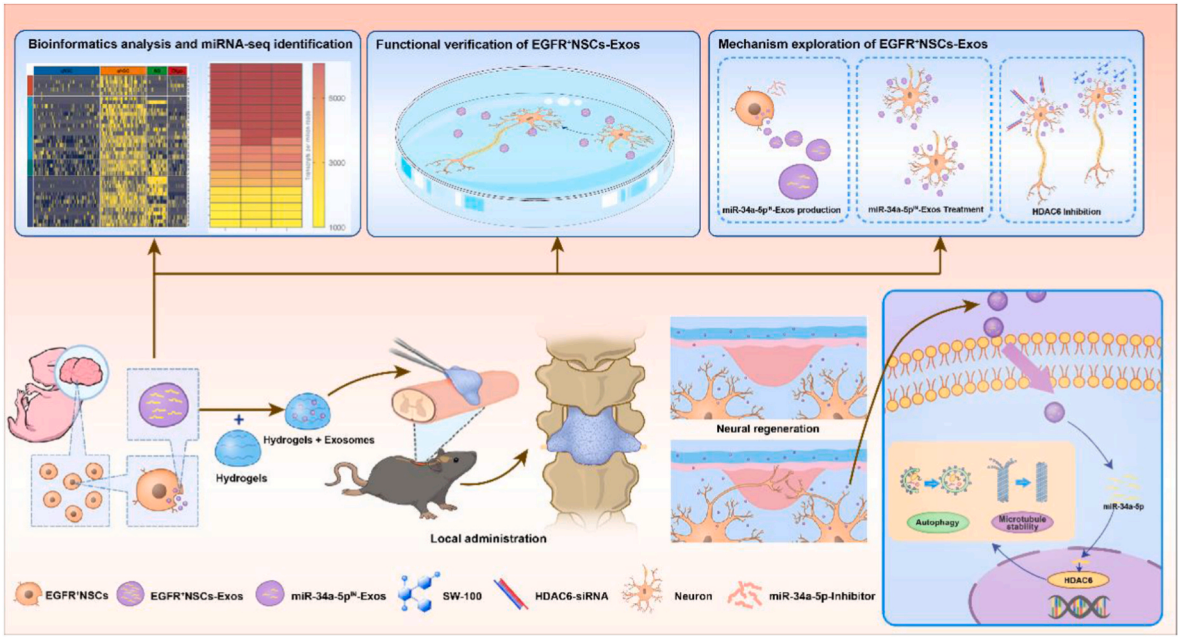

Fig. 1. Schematic of the project.
In this study, we have identified a specific subtype of neural stem cells (NSCs) known as EGFR$^+$NSCs and isolated their exosomes. By employing transcriptomic and miRNA profiling, we characterized both EGFR$^+$NSCs and their exosomes. Using an in vitro cellular model, we explored the mechanisms through which exosomes derived from EGFR$^+$NSCs promote axonal outgrowth. In conjunction with 3D printing technology and a hydrogel scaffold, we designed and implemented a hydrogel-coated exosomal patch for the treatment of SCI, demonstrating superior efficacy in enhancing neural regeneration. These results showed that the exosomes derived from EGFR$^+$NSCs were found to deliver miR-34a-5p to neurons, resulting in the downregulation of HDAC6. This, in turn, activated the autophagy process and enhanced microtubule stabilization. Our study introduces a novel class of exosomes derived from EGFR$^+$NSCs with the potential to enhance functional recovery following SCI, offering a promising cell-free therapy approach for SCI treatment.

3.2. The exosomes obtained from EGFR$^+$ NSCs promoted better functional recovery in mice with spinal cord injury

To effectively maintain the action concentration of local exosomes after spinal cord injury, the photo-cured hydrogel base on the GelMA and HA-NB was used to embed exosomes. Firstly, we characterized the physicochemical properties of the hydrogel, the SEM image of the sol-gel transformation after UV suggested that the porous hydrogel is a good exosome carrier (Fig. 3A). And the cytocompatibility test did not show any significant toxicity to neuron cells (Fig. 3B). We also found that the hydrogel treatment did not result in appreciable cardiotoxicity, hepatotoxicity, spleen cell toxicity, pulmonary toxicity, and nephrotoxicity by HE staining (Figs. S1A–E). These results demonstrated that the photo-cured hydrogel exhibited good biocompatibility. As illustrated in Fig. 3C, the hydrogel degraded by approximately 70 % after 28 days in vitro analysis. The results of the swelling test showed that the hydrogel showed rapid swelling behavior within 24 h, and the swelling rate reached nearly 1200 % (Fig. 2D). The release curve demonstrated a continuous release of loaded exosomes from the hydrogel, reaching approximately 80 % of the cumulative amount after 28 days (Fig. 3E). Next, we used confocal multi-layer 3D scanning to visualize the PKH67-labeled exosomes retained within the hydrogel. The results demonstrated that primary NSCs-Exos and EGFR$^+$NSCs-Exos were uniformly distributed in hydrogel (Fig. 3F). Exosome-loaded hydrogels were printed into 2*2*0.5 mm-sized patches based on the shape of removed lamina using 3D printing technology and placed over the injury lesion in spinal cord injured mice (Fig. S1F). Using in vivo imaging techniques to assess the release of hydrogel-coated exosomes, we found that most DIR signal was detected at the 10 mg/mL group 7 days post-implantation (Figs. S3A–B). The DIR signal was still retained within the spinal cord injury zone 14 days post-SCI (Fig. 3G–H). To confirm that the hydrogel patch was maintained on the surface of the spinal cord, we obtained the spinal cord tissues 3, 7 and 14 days after the injury respectively, and found that even 14 days after the injury, some hydrogel remained on the surface of the spinal cord (some degraded), indicating that the current molding method could ensure the fixation of the hydrogel patch within 14 days (Figs. S1G–H). BMS scores and BMS sub-scores were evaluated preoperation and on days 0, 1, 3, 7, 14, 21, and 28 post-SCI after the treatment of Primary NSCs-Exos or the EGFR$^+$NSCs-Exos. All groups' functional behavior deteriorated following SCI. However, in comparison to the control group, the group treated with primary NSCs-Exos displayed a significant improvement in post-SCI motor dysfunction. Furthermore, the EGFR$^+$NSCs-Exos group demonstrated an even better functional recovery when compared to the primary NSCs-Exos group (Fig. 3I–J). Additionally, the motor-evoked potentials (MEPs) were analyzed, and the results showed that at 28 days post-SCI and the results revealed that the amplitude of primary NSCs-Exos treated mice had significantly increased compared to the control mice treated with vehicles at day 28 post-SCI (Fig. 3K-L). Histological investigation with H&E staining was carried out to further determine the therapeutic benefits of NSCs-Exos on neurological functional recovery after SCI. It was demonstrated that 28 days after SCI, the injured area was noticeably less in the primary NSCs-Exos treated animals than in the mice that had received vehicle treatment (control groups). Additionally, mice treated with EGFR$^+$NSCs-Exos had fewer lesion areas than those treated with primary NSCs-Exos (Figs. S2A–B). The bladder's function assessment following SCI was consistent with the histological evaluation (Figs. S2C–D). These data provide evidence that the mice in the EGFR$^+$NSCs-Exos group had better functional recovery as compared to the primary NSCs-Exos.

3.3. EGFR$^+$ NSCs-derived exosomes promoted neural regrowth both in vivo and in vitro

To identify the cellular mechanisms underlying functional recovery after SCI, exosomes were labeled with PKH67 dye and embedded in the

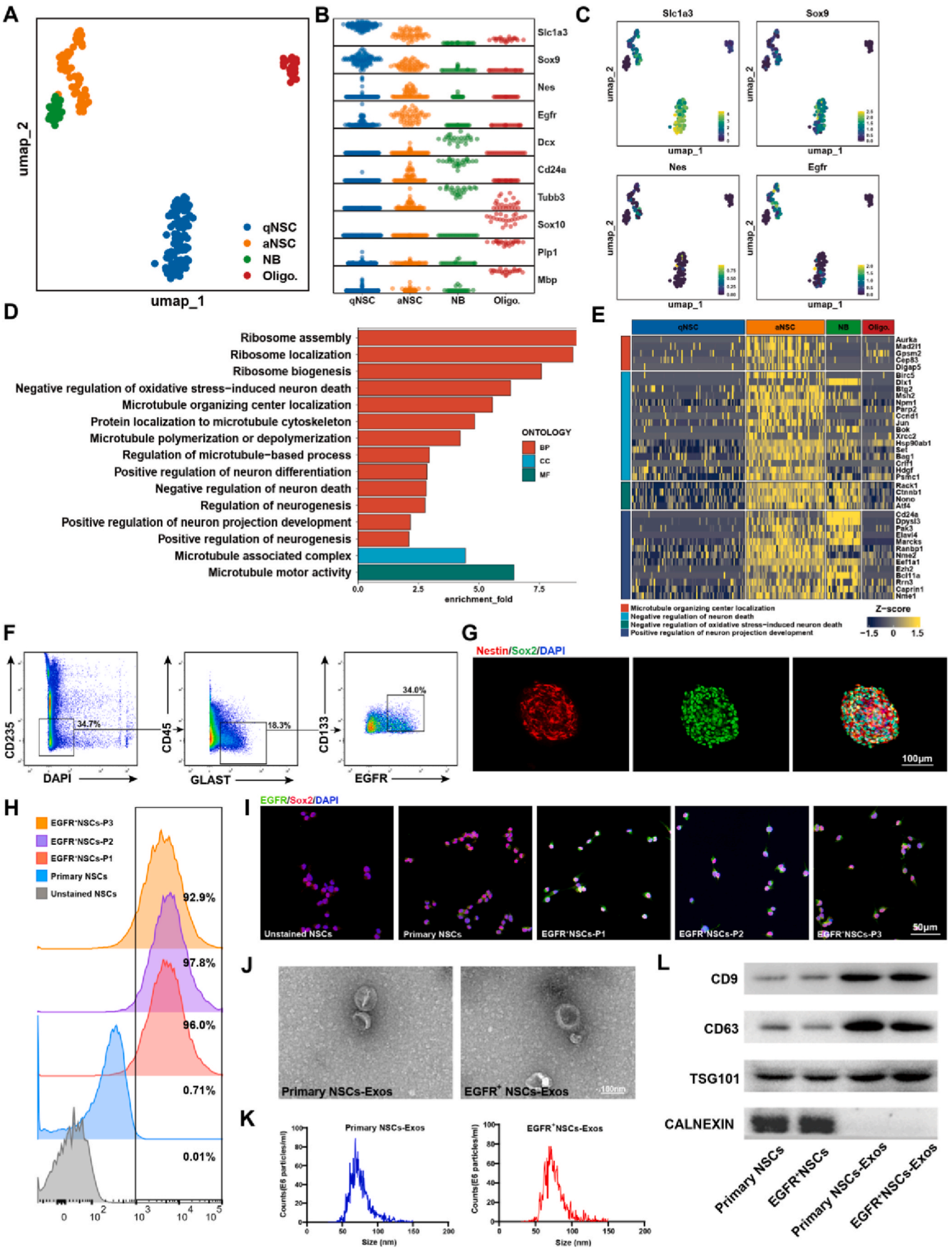

(caption on next page)

Fig. 2. Characteristics of single-cell Transcriptome of neural stem cells and identification of their exosomes.
(A) Uniform Manifold Approximation and Projection (UMAP) of the cells from mice SVZ. Colors indicate assigned activation states and cell types. (B) Violin plots showing the course of expression for genes in the neurogenic lineage (NSCs and neuroblasts). (C) Expression distribution of selected marker genes. (D) Selected GO biological processes were significantly overrepresented in aNSCs subtype ranked by enrichment foldchange. (E) Average expression of selected marker genes in (D) for each cell type in (A). (F) Flow cytometry sorting of the living $CD235^{-}CD45^{-}CD133^{+}EGFR^{+}$NSCs. (G) Identification of $EGFR^{+}$NSCs using immunofluorescent analyses of the expression of specific stem cell markers Nestin and Sox2, scale bar, 100 μm. (H) Flow cytometry analysis of EGFR as a cell marker. The unstained blank control is shown as a grey dashed curve and the test sample is shown as the blue, red, pink and orange curve. (I) immunofluorescent analyses of the expression of EGFR in the passaged NSCs. scale bar, 50 μm. (J) TEM image of exosomes secreted by primary and $EGFR^{+}$NSCs, scale bar, 100 nm. (K) Nanoparticle tracking analysis of exosomes isolated from primary NSCs and $EGFR^{+}$NSCs. (L) Western blotting analysis of exosome-specific markers CD9, CD63, and TSG101, as well as the negative exosomal marker CALNEXIN.

photo-cured hydrogel. 24 h post SCI, fluorescence microscopy was used to detect the exosomal absorption. As shown in Fig. S3A, we discovered that exosomes produced by primary and $EGFR^{+}$NSCs could infiltrate the blood-brain barrier (BBB) after administered and be taken up by neurons and phagocytes around the lesion side, while rarely absorbed by astrocytes, stem cells and endothelial cells (Figs. S4B–E). Consistent with the previous functional assessment, we also detected robust neurite regrowth in the $EGFR^{+}$NSCs-Exos group using anti-GAP43 and anti-NF immunofluorescent labeled neural axons (Fig. 3M – P). To confirm the therapeutic effects of $EGFR^{+}$NSCs-Exos on neural regeneration in SCI treatment, the cerebral neurons were isolated and cultured as a cell model to investigate the bioactivity of the NSCs-derived exosomes. Using SND450 neural culture plates to isolate neuronal cytoplasm and axons, the distal axons were severed to simulate axonal rupture after spinal cord injury. The axonal regenerative assay revealed that the $EGFR^{+}$NSCs-Exos promotes axonal regrowth in a dose-dependent manner (Figs. S3A–B). However, simple administration of the Primary NSCs-Exos and $EGFR^{+}$NSCs-Exos could not further promote neurite growth, and the neurons in the stable culture condition did not show the capability to absorb the additional NSCs-Exos and $EGFR^{+}$NSCs-Exos (Figs. S4F–H). Simulating the microenvironment of neurite growth inhibition, we used chondroitin sulfate (CSPG) to intervene in the cultured neurons. Under the condition of CSPG administration, the neurites stained with Tuj1 showed an inhabitation of neurite outgrowth (Figs. S4I–J). It was found that the PKH67 labeled NSCs-Exos and $EGFR^{+}$NSCs-Exos could be taken up by neurons treated with CSPG (Fig. S4K). Quantitative measurements revealed that, after exosomal treatment, the cortical neurons featured an elongated neurite, and the $EGFR^{+}$NSCs-Exos have a stronger capability for alleviating the inhibitory effects of CSPG on neurite growth (Fig. 3Q-R). To further cultivate neurons derived from the spinal cord, we employed CSPG intervention to mimic the environment of growth inhibition. We discovered that $EGFR^{+}$NSCs-Exos also possessed a superior capability in promoting spinal cord neuron regeneration (Fig. S2L-M). The axonal regenerative assay revealed that the $EGFR^{+}$NSCs-Exos also exhibited a stronger ability to promote axonal regeneration (Fig. 3S-T). These findings indicated that, compared to primary NSCs-Exos, the $EGFR^{+}$NSCs-Exos has a stronger capability for triggering neural regeneration, according to both in vivo and in vitro evidence.

3.4. *miR-34a-5p was enriched in $EGFR^{+}$NSCs-Exos and could deliver to neurons*

Exosomes play a vital role, mainly dependent on their internal contents. First, we examined the transmission of EGFR in exosomes derived from $EGFR^{+}$NSCs and found that EGFR expression was relatively low in the $EGFR^{+}$NSCs-Exos (Fig. S5A). Additionally, we assessed the expression levels of EGFR in neurons following $EGFR^{+}$NSCs-Exos intervention and observed that exosomal intervention did not lead to an increase in EGFR levels in neuronal cells (Figs. S5B–C). One of the key cargos for mediating the biological function of exosomes is miRNA. Both in vivo and in vitro studies have revealed that $EGFR^{+}$NSCs-derived exosomes have a stronger capability for promoting neurite outgrowth compared to the primary NSCs derived exosomes. Therefore, the total RNA was extracted from the $EGFR^{+}$NSCs-Exos, and analyzed using microRNA sequencing. The miRNA-seq demonstrated that a total of 1143 miRNAs were screened (Table S2), and the top 20 expressed miRNAs were listed in the heatmap (Fig. 4A). Among these highly expressed miRNAs, the top 10 miRNAs were quantified using qRT-PCR between primary and $EGFR^{+}$NSCs-Exos. Among them, miR-34a-5p showed abundant expression in $EGFR^{+}$NSCs-Exos and had 10-fold greater levels than in primary NSCs-Exos (Fig. 4B). To determine the role of miR-34a-5p in mediating neural regrowth, the miR-34a-5p mimic and miR-34a-5p inhibitor were administrated to cultured cortical neurons. It was demonstrated that mimics of miR-34a-5p alleviated the inhibitory effects of CSPG on neurite growth, and the miR-34a-5p-inhibitor offset the ability of $EGFR^{+}$NSCs-Exos for promoting neurite growth (Fig. 4C–D). The axonal regenerative assay also revealed the vital role of miR-34a-5p in promoting neural axonal regrowth (Fig. 4E–F). In the meantime, we found a significant increase of miR-34a-5p level in neurons in spinal cord injured tissue after administration with $EGFR^{+}$NSCs-Exos (Fig. 4G–H). The qRT-PCR result also revealed that the $EGFR^{+}$NSCs-Exos upregulated the miR-34a-5p expression in cultured neurons (Fig. 4I) without influencing the pri-miR-34a-5p expression (Fig. 4J), which indicated that the expression of the mature miR-34a-5p in cultured neurons was delivered from the $EGFR^{+}$NSCs-Exos. These results indicated that the $EGFR^{+}$NSCs-Exos can transfer exosomal miR-34a-5p to the target neuron cells and affect their bioactivity.

3.5. *miR-34a-5p mediated the effect of $EGFR^{+}$NSCs-Exos on promoting neurological functional recovery and neurite regrowth*

To further investigate the mechanistic insight into the role of exosomal miR-34a-5p in mediating the positive effect of $EGFR^{+}$NSCs-Exos on promoting neurological functional recovery and neurite regrowth following SCI, we constructed miR-34a-5p knockdown $EGFR^{+}$NSCs using miR-34a-5p-inhibitor, along with negative control of miR-34a-5p as a control. Exosomes were isolated from $EGFR^{+}$NSCs and miR-34a-5p knockdown $EGFR^{+}$NSCs, respectively. miR-34a-5p expression was lower in exosomes derived from miR-34a-5p-knockdown $EGFR^{+}$NSCs (named miR-34a-$5p^{IN}$-Exos) than exosomes derived from negative control of miR-34a-5p treated $EGFR^{+}$NSCs (named NC-Exos) (Fig. 5A). As illustrated in Fig. 5B–C, the downregulation of miR-34a-5p in $EGFR^{+}$NSCs-Exos could eliminate the effects of functional recovery noticed by NC-Exos treatment. Electrophysiological analysis of MEPs showed that the miR-34a-$5p^{IN}$-Exos treated mice show lower amplitude and longer latent period than the NC-Exos treated mice (Fig. 5D–E). The histological investigation with H&E staining showed that the knockdown of miR-34a-5p could offset the effects of NC-Exos in reducing the injury area (Figs. S6A–B), indicating that $EGFR^{+}$NSCs-Exos promotes functional behavior recovery via transfer miR-34–5p into the neuron. We then evaluated the functional role of exosomal miR-34–5p derived from $EGFR^{+}$NSCs in the mediation of neurite regrowth in vivo. As shown in Fig. 5F–I, administering miR-34a-$5p^{IN}$-Exos attenuated the neurite

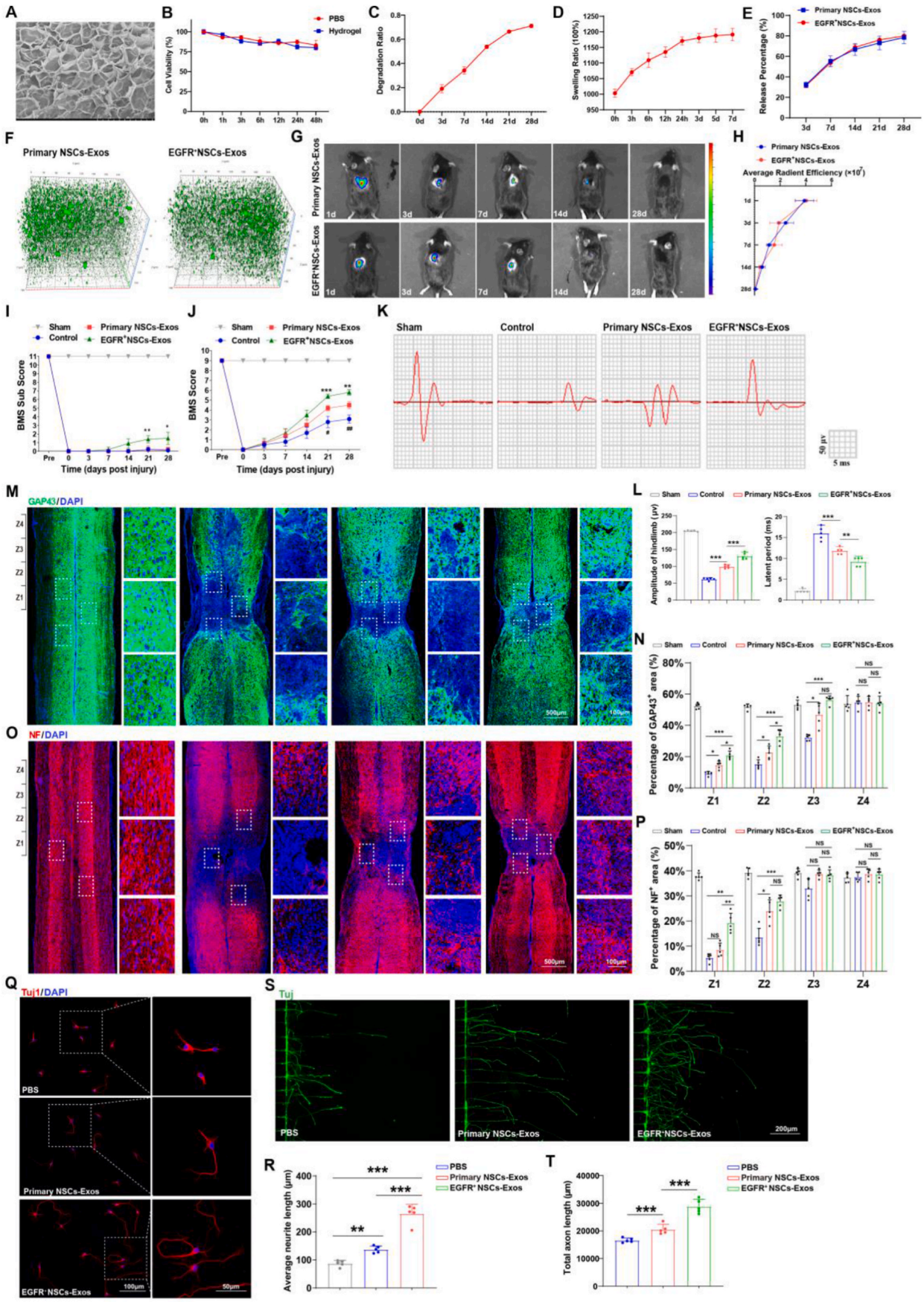

(caption on next page)

Fig. 3. EGFR $^{+}$ NSCs-derived exosomes promoted functional recovery and neural remodeling both in vivo and in vitro.
(A) SEM images showed the microstructures of the hydrogel. Scale bar: 50 μm. (B) The survival and cell viability of neurons co-incubated with hydrogel, were detected by the CCK-8 assay. N = 3 per group. (C) In vitro degradation curves of hydrogels over time based on gravimetric measurements. N = 3 per group. (D) Swelling ratios of hydrogels over time. (E) Release curves of Exosomes at different time points. N = 3 per group. (F) Confocal multi-layer scanning and 3D reconstruction of PKH67-labeled exosomes retained within the hydrogel. (G) In vivo tracing of the distribution of DiR-labeled exosomes embedded in hydrogels in the injured spinal cord at 1, 3, 7, 14, and 28 days post-SCI. (H) Quantification of average fluorescence efficiency of (G). N = 3 per group. (I) BMS scores in sham, control, Primary NSCs-Exos, and EGFR^{+}NSCs-Exos–treated groups at different time points post-SCI. N = 5 per group. * Control vs Primary NSCs-Exos, # Primary NSCs-Exos vs EGFR^{+}NSCs-Exos. (J) BMS sub scores in sham, control, Primary NSCs-Exos, and EGFR^{+}NSCs-Exos treated groups at different time points post-SCI. N = 5 per group. (K) Representative electrophysiological trace images were recorded in each group at 28 days post-SCI. (L) Measurement of the MEP amplitude and latent period in (K). (M) Representative immunofluorescent stains of GAP43 images of the spinal cord at 28 days post-injury in each group. The Z1-Z4 indicates the area sequential 500 μm roster to the epicenter. Scale bar, 500 μm. (N) Quantification of GAP43 positive signals in different areas roster to the epicenter of sham, control, primary NSCs-Exos, and EGFR^{+}NSCs-Exos treated mice in (M). (O) Representative immunofluorescent stains of NF images of the spinal cord at 28 days post-injury in each group. The Z1-Z4 indicates the area sequential 500 μm roster to the epicenter. Scale bar, 500 μm. (P) Quantification of NF positive signals in different areas roster to the epicenter of sham, control, primary NSCs-Exos, and EGFR^{+}NSCs-Exos treated mice in (O). (Q) Representative immunofluorescent stains of Tuj1 image of the cultured neurons of PBS, primary NSCs-Exos, and EGFR^{+}NSCs-Exos treated groups. scale bar, 100 μm and 50 μm. (R) Quantification of Tuj1 positive neurite length in PBS, primary NSCs-Exos, and EGFR^{+}NSCs-Exos treated neurons in (Q). (S) Representative immunofluorescent images of the regenerative axons on the microfluidic culture plate (green: Tuj1). (T) Quantification of total axonal length in (S). N = 5 per group. Data are presented as mean ± SD, NS, no significant difference, $^{*}P < 0.05$, $^{**}P < 0.01$, $^{***}P < 0.001$.

regrowth besides the lesion core and decreased the amount of GAP43 and NF positive signal in spinal cord sections compared to the NC-Exos groups. It was shown that NC-Exos alleviated the inhibitory effects of CSPG on neurite growth, while the beneficial effects were abolished by miR-34-5p^{IN}-Exos administrating (Figs. S6C–D). Similarly, the neural axonal regrowth assay showed that the miR-34a-5p inhibition weakened the therapeutic effect of EGFR^{+}NSCs-Exos (Fig. 5J–K). Collectively, these results demonstrated that miR-34–5p is essential for the EGFR^{+}NSCs-Exos in promoting neurite regrowth.

3.6. EGFR $^{+}$ NSCs-Exos-derived miR-34a-5p promoted the neurite regrowth and reduces HDAC6 expression

To further explore the targeted regulated molecular mechanisms of exosomal miR-34a-5p secreted by EGFR^{+}NSCs in modulating the neurite regrowth, the bioinformatic tools: miRDB and microT were combined used to identify a putative target gene of miR-34a-5p. According to the online database of miRNA target genes and the GO term-0030,517 (negative regulation of axon extension), we identified four potential target genes of the miR-34a-5p, including the *Aatk*, *Sema4b*, *Ntn1* and *HDAC6* (Fig. 6A). Among the target genes, the histone deacetylases 6 (HDAC6) is the only HDAC localized in the cytoplasm, which can regulate the deacetylation of nonhistone structures such as autophagy and deacetylase of microtubules. To verify, which could be significantly inhibited after administrating with EGFR^{+}NSCs-Exos, the expression level of *HDAC6* in cultured neurons was the most significantly down-regulated gene among these genes (Fig. 6B). The luciferase reporter experiment was used to determine if the *HDAC6-3′UTR* is a direct target for miR-34a-5p, we found that miR-34a-5p mimics dramatically decreased the luciferase activity of the wild type (WT), while the luciferase activity of the mutant type (Mut) of 3′UTR reporter constructs was not altered (Fig. 6C). These results indicated that miR-34a-5p could directly bind to the 3′UTR of *HDAC6* and repress its expression. The immunofluorescent staining and western blotting confirmed that EGFR $^{+}$ NSCs-Exos could significantly reduce the HDAC6 expression in cultured neuron cells (Fig. 6D–G). For verifying the effects of EGFR $^{+}$ NSCs-Exos on regulating HDAC6 expression, the NC-Exos and miR-34-5p^{IN}-Exos treated mice were satisfied for HDAC6 expression detection. The results showed that the mice in NC-Exos treated groups demonstrated a lower HDAC6 expression level in neurons, as revealed by immunofluorescent as compared with the control groups, and these effects were reversed followed by miR-34a-5p inhibited (Fig. 6H and J). Similar results of HDAC6 expression change trend followed by miR-34a-5p inhibition were also observed by Western blot analysis (Fig. 6I and K). Collectively, our findings indicated that EGFR^{+}NSCs-Exos derived miR-34a-5p promoted neurite regrowth and reduced the HDAC6 expression in neurons.

3.7. miR-34a-5p mediated the effect of EGFR^{+}NSCs-Exos on regulating neural microtubule stabilization and autophagy induction

By analyzing the expression level of the miR-34a-5p in neurons in the spinal cord injured section, we can see notable upregulated expression of miR-34a-5p in neurons with the treatment of NC-Exos, as compared with the control groups. However, these effects were attenuated following the inhibition of miR-34a-5p (Fig. 7A and C). As HDAC6 was reported to regulate neural microtubule stability and neural autophagy in axonal regeneration [46–48], the expression of acetylated and tyrosinated α-tubulin, as well as autophagy-related proteins in the injured tissue, was analyzed using immunofluorescent staining and western blotting. The results of the study revealed that the administration of NC-Exos increased the A/T ratio, indicating improved stability. Meanwhile, inhibition of exosomal miR-34–5p decreased microtubule stiffness (Fig. 7B and D, Fig. 7G and H). Meanwhile, NC-Exos were found to have the capability to enhance the expression of autophagy-related proteins LC3 expression in neurons as evidenced by immunofluorescence via miR-34a-5p when compared with the control group (Fig. 7E–F). Similar results were found in the Western blot experiment, the LC3A/B and Beclin1 were increased expression in the NC-Exos treatment groups as compared to the control groups, while the P62 as an autophagy negative regulator was downregulated. After treatment with miR-34-5p^{IN}-Exos, there was a marked decline in the protein level expression of LC3A/B and Beclin1, along with the upregulation of autophagy arresting P62 (Fig. 7G and I). The results of immunohistochemistry also indicated miR-34a-5p which was highly expressed in EGFR^{+}NSCs-Exos is required and essential for mediating the function of exosome on microtubules stabilization and neural autophagy (Figs. S7A–C).

3.8. EGFR $^{+}$ NSCs-Exos stabilized the microtubules and activated autophagy via the miR-34a-5p/HDAC6 pathway

To further determine the role of miR-34a-5p/HDAC6 in the mediating effect of EGFR^{+}NSCs-Exos on promoting neurite regrowth, we generated miR-34a-5p^{IN}-Exos and HDAC6 siRNA to reveal the role of miR-34a-5p/HDAC6 in regulating neural regrowth. As evidenced by the neurite and neural axonal regrowth assay, the promoting effects of EGFR^{+}NSCs-Exos were suppressed by miR-34a-5p silencing. However, the inhibition of HDAC6 restored the promotion effects of EGFR^{+}NSC-

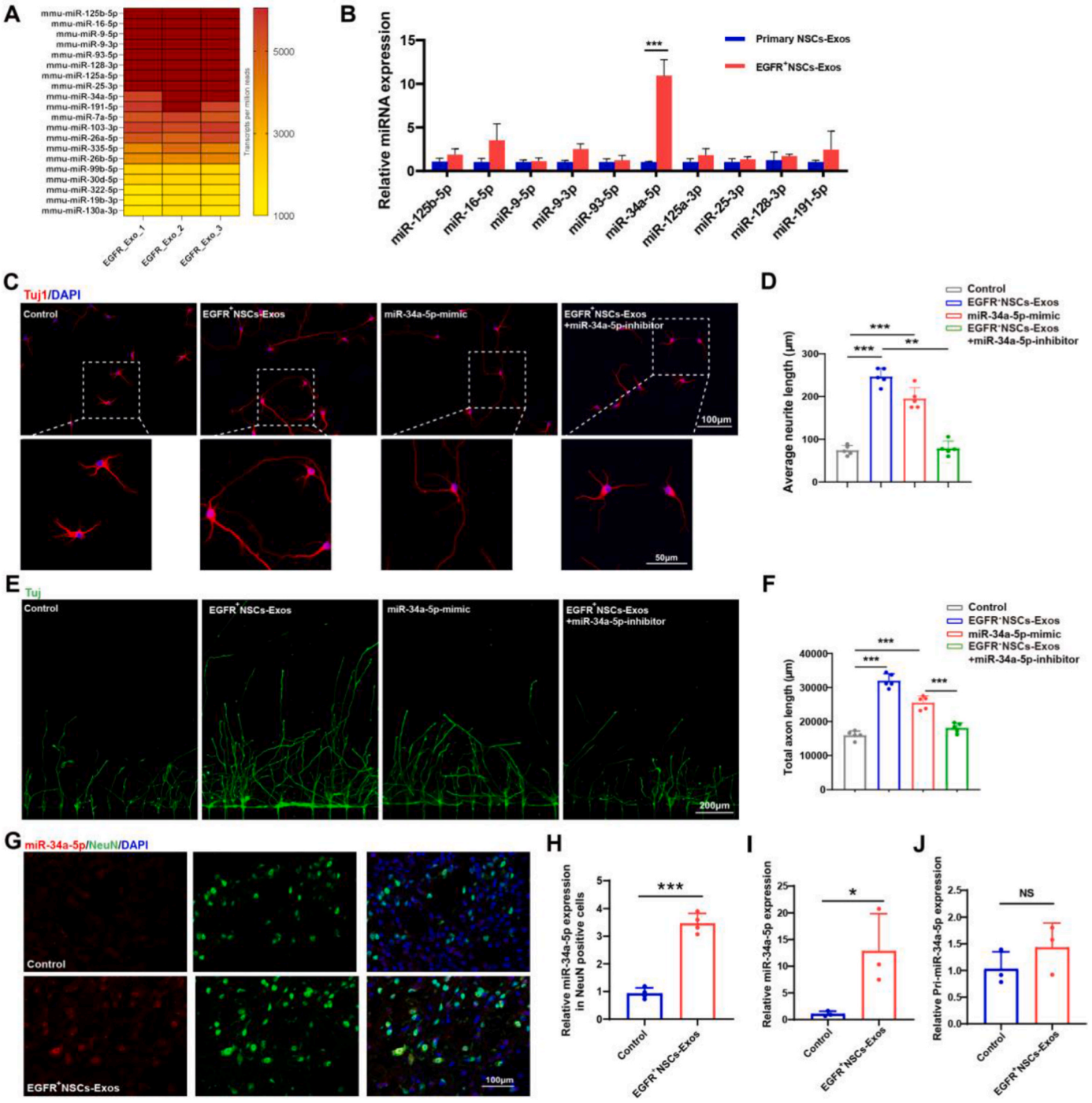

Fig. 4. miR-34a-5p was enriched expression in EGFR$^+$NSCs derived exosomes and could deliver to spinal neurons.
(A) miRNAs expression pattern in EGFR$^+$NSCs-Exos. (B) Quantitative analysis of the top 10 expressed miRNAs in EGFR$^+$NSCs-Exos between the Primary NSCs-Exos and EGFR$^+$NSCs-Exos by qRT-PCR analysis. N = 5 per group. (C) Representative immunofluorescent stains of Tuj1 image of the cultured neurons of PBS, EGFR$^+$NSCs-Exos, miR-34a-5p mimic, and EGFR$^+$NSCs-Exos + miR-34a-5p-inhibitor-treated groups. scale bar, 100 μm. (D) Quantification of Tuj1 positive neurite length in (C). N = 5 per group. (E) Representative immunofluorescent images of the regenerative axons on the microfluidic culture plate (green: Tuj1). (F) Quantification of total axonal length in (E). N = 5 per group. (G) Representative fluorescence in situ hybridization image of the spinal cord tissue of the control and EGFR$^+$NSCs-Exos treated mice. Neun (green), miR-34a-5p (red), scale bar, 100 μm. (H) Quantification of miR-34a-5p immunofluorescent intensity of the NeuN positive cells in (G). (I) Quantitative analysis of the mature miR-34a-5p in control and EGFR$^+$NSCs-Exos treated neurons. (J) Quantitative analysis of the Pri-miR-34a-5p in control and EGFR$^+$NSCs-Exos treated neurons. Data are presented as mean ± SD, NS, no significant difference, $^*P < 0.05$, $^{**}P < 0.01$, $^{***}P < 0.001$.

Exos (Fig. 8A–B and Figs. S8A–B). The fluorescent staining of markers Ace-tub and Tyr-tub was administrated to evaluate microtubule stability, the results showed that HDAC6 knockdown upregulated the A/T ratio, reversed the effects of miR-34a-5p^{IN}-Exos (Fig. 8C–D). The autophagy detected assay and TEM results also showed the HDAC6 knockdown in neurons rescued the autophagy flux following the miR-34a-5p^{IN}-Exos treatment (Fig. 8E–G). Furthermore, we performed western blotting to detect autophagy-relative proteins (LC3A/B, Beclin1 and P62) and microtubule stability markers (Ace-tub and Tyr-tub) of the aforementioned treatment groups, and the results were consistent with

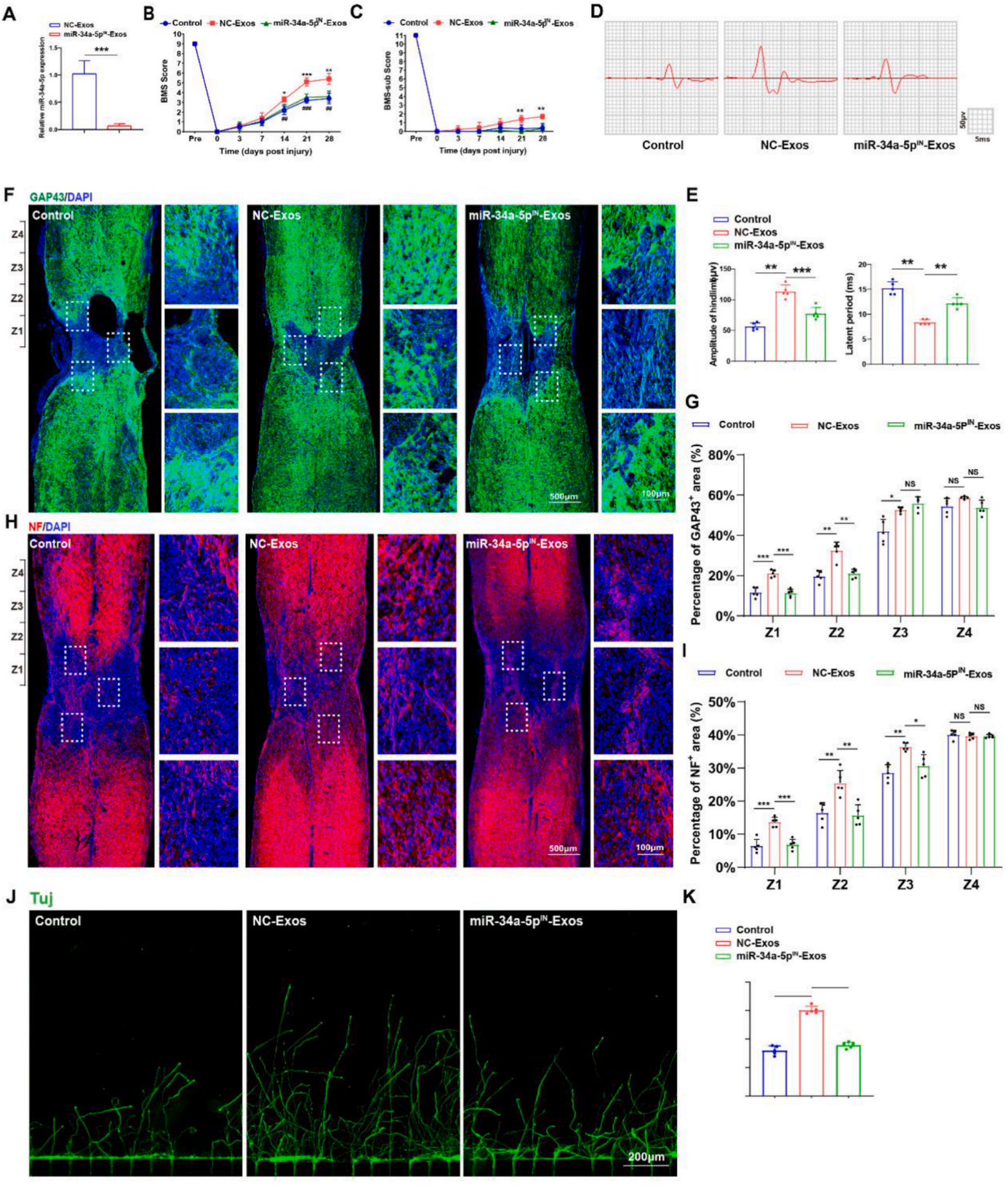

(caption on next page)

Fig. 5. miR-34a-5p mediated the effects of EGFR^{+}NSCs-Exos on neurological functional recovery and neural regrowth.
(A) Quantitative analysis of the miR-34a-5p expression in the miR-34a-5p-inhibitor and miR-34a-5p-NC administrated EGFR^{+}NSCs-derived exosomes. (B) BMS scores in control, NC-Exos, and miR-34a-5p^{IN}-Exos groups at different time points post-SCI. N = 5 per group. * NC-Exos vs miR-34a-5p^{IN}-Exos, # control vs NC-Exos. (C) BMS sub scores in control, NC-Exos, and miR-34a-5p^{IN}-Exos groups at different time points post-SCI. N = 5 per group. (D) Representative electrophysiological trace images were recorded in each group at 28 days post-SCI. (E) Measurement of the MEPs, amplitude, and latent period in (D). N = 5 per group. (F) Representative immunofluorescent stains of GAP43 images of the spinal cord at 28 days post-injury in each group. The Z1-Z4 indicates the area sequential 500 μm roster to the epicenter. Scale bar, 500 μm. (G) Quantification of GAP43 positive signals in different areas roster to the epicenter of control, NC-Exos, and miR-34a-5p^{IN}-Exos groups in (F). N = 5 per group. (H) Representative immunofluorescent stains of NF images of the spinal cord at 28 days post-injury in each group. The Z1-Z4 indicates the area sequential 500 μm roster to the epicenter. Scale bar, 500 μm. (I) Quantification of NF positive signals in different areas roster to the epicenter of control, NC-Exos, and miR-34a-5p^{IN}-Exos groups in (H). N = 5 per group. (J) Representative immunofluorescent images of the regenerative axons on the microfluidic culture plate (green: Tuj1). (K) Quantification of total axonal length in (J). N = 5 per group. Data are presented as mean ± SD, NS, no significant difference, $^{*}/^{\#}P < 0.05$, $^{**}/^{\#\#}P < 0.01$, $^{***}/^{\#\#\#}P < 0.001$.

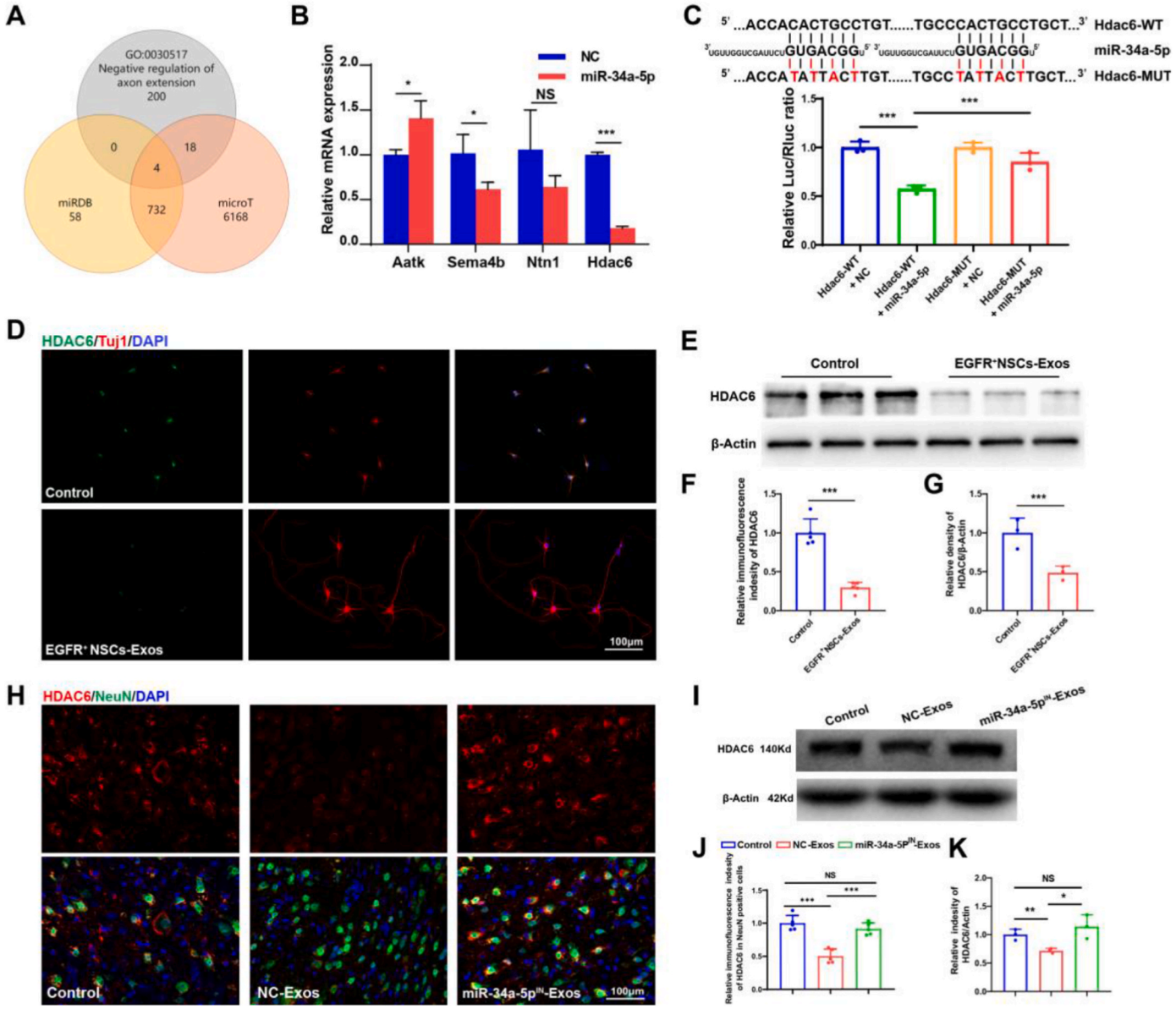

Fig. 6. EGFR $^{+}$ NSCs-Exos derived miR-34a-5p directly downregulated HDAC6 expression.
(A) The Venn diagram demonstrated the potential target genes of exosomal miR-34a-5p. (B) Quantitative analysis of the four potential target genes of miR-34a-5p using qRT-PCR. N = 3 per group. (C) Complementary sequences between miR-34a-5p and the 3′UTR of HDAC6 and relative luciferase activities of the HDAC6-wild type (WT) + negative control (NC) group, HDAC6-WT + miR-34a-5p group, HDAC6-MUT + NC group, and HDAC6-MUT + miR-34a-5p group. N = 3 per group. (D) Representative immunofluorescent stains of HDAC6 and Tuj1 images of cultured neurons after administrating with the miR-34a-5p. (E) Western blot analysis of HDAC6 in control and EGFR^{+}NSCs-Exos treated groups. (F) Quantification of HDAC6 expression in (E). N = 5 per group. (G) Quantification of the relative expression of HDAC6 in (E). N = 3 per group. (H) Representative immunofluorescent stains of HDAC6 and Neun images in spinal cord injured samples from control, EGFR^{+}NSCs-Exos, and miR-34a-5p^{IN}-Exos groups. (I) Western blot analysis of HDAC6 in injured spinal cord tissues from control, EGFR^{+}NSCs-Exos, and miR-34a-5p^{IN}-Exos groups. (J) Quantification of HDAC6 expression in (H). N = 5 per group. (K) Quantification of HDAC6 expression in (I). N = 3 per group. Data are presented as mean ± SD; NS, no significant difference; $^{*}P < 0.05$, $^{**}P < 0.01$, and $^{***}P < 0.001$.

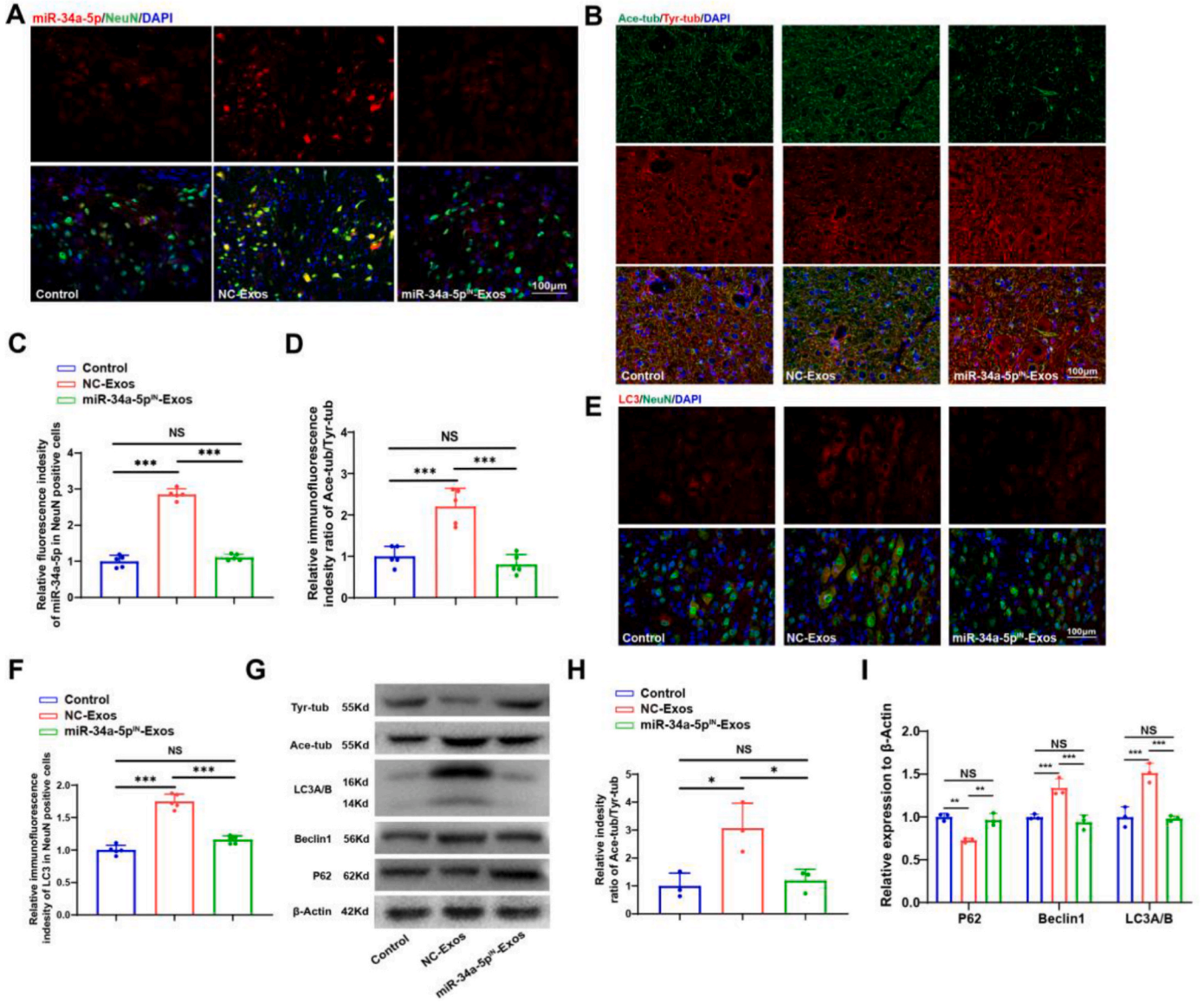

Fig. 7. EGFR $^{+}$ NSCs-Exos regulated the microtubule stabilization and activation of autophagy via miR-34a-5p.
(A) Representative fluorescence in situ hybridization image of the spinal cord tissue of the control, NC-Exos, and miR-34a-5p^{IN}-Exos treated mice. Neun (green), miR-34a-5p (red), scale bar, 100 μm. (B) Immunofluorescence staining of Ace-tub and Tyr-tub on spinal cord injury tissue from control, NC-Exos and miR-34a-5p^{IN}-Exos treatment groups, Scale bars, 100 μm. (C) Quantification of miR-34a-5p immunofluorescent intensity of the NeuN positive cells in (A). N = 5 per group. (D) Quantification of the relative expression of Ace-tub to Tyr-tub in (B). N = 5 per group. (E) Immunofluorescence staining of LC3 and Neun in spinal cord injured sample from each group. (F) Quantification of the relative expression of LC3 in (E). N = 5 per group. (G) Western blot analysis of Ace-tub, Tyr-tub, and autophagy-related proteins LC3A/B, Beclin1, and the P62 in various treated groups. (H) Quantification of acetylated to tyrosinated α-tubulin ratio in (G). (I) Quantification of autophagy-related protein expression in (G), N = 3. Data are presented as mean ± SD; NS, no significant difference; $^{*}P < 0.05$, $^{**}P < 0.01$, and $^{***}P < 0.001$.

the fluorescence staining data (Fig. 8H–K). These data indicated that EGFR^{+}NSCs-Exos promotes neural regrowth via miR-34a-5p/HDAC6 pathway by mediating microtubule stabilization and autophagy activation.

3.9. EGFR $^{+}$ NSC-Exos promoted functional recovery post SCI via miR-34a-5p/HDAC6 pathway

To investigate whether miR-34a-5p/HDAC6 is involved in EGFR^{+}NSC-Exos mediation of recovery SCI. miR-34a-5p^{IN}-Exos and SW-100 (a selective HDAC6 inhibitor) were combined and administrated to SCI mice [49]. The immunofluorescent and immunohistochemistry staining of the spinal cord sections showed that the miR-34a-5p inhibition attenuated the microtubule acetylation and neural autophagic activation around the lesion core. and the further SW-100 administration reversed the effects of miR-34a-5p inhibition (Figs. S9A–F). BMS and BMS sub-scores evaluation demonstrated that miR-34a-5p^{IN}-Exos administration attenuated the positive effect of neuroprotection with the EGFR^{+} NSCs-Exos. However, the presence of SW-100 could rescue the functional effects of miR-34a-5p^{IN}-Exos on enhancing neurological functional recovery as compared to the miR-34a-5p^{IN} -Exos treated alone (Fig. 9A–B). The electrophysiological analysis confirmed the significant effects of the miR-34a-5p/HDAC6 pathway in regulating the neurologic connectivity recovery of the EGFR^{+}NSC-Exos treated mice (Fig. 9C–D). The H&E staining also demonstrated that silence of HDAC6 by SW-100 can abolish the inhibitory role of miR-34a-5p^{IN}-Exos on suppressing the injured spinal cord tissue healing after SCI (Figs. S10A–B). In addition, the bladder functional analysis after SCI showed the same results as the neurological functional test (Figs. S10C–D). The immunofluorescent staining

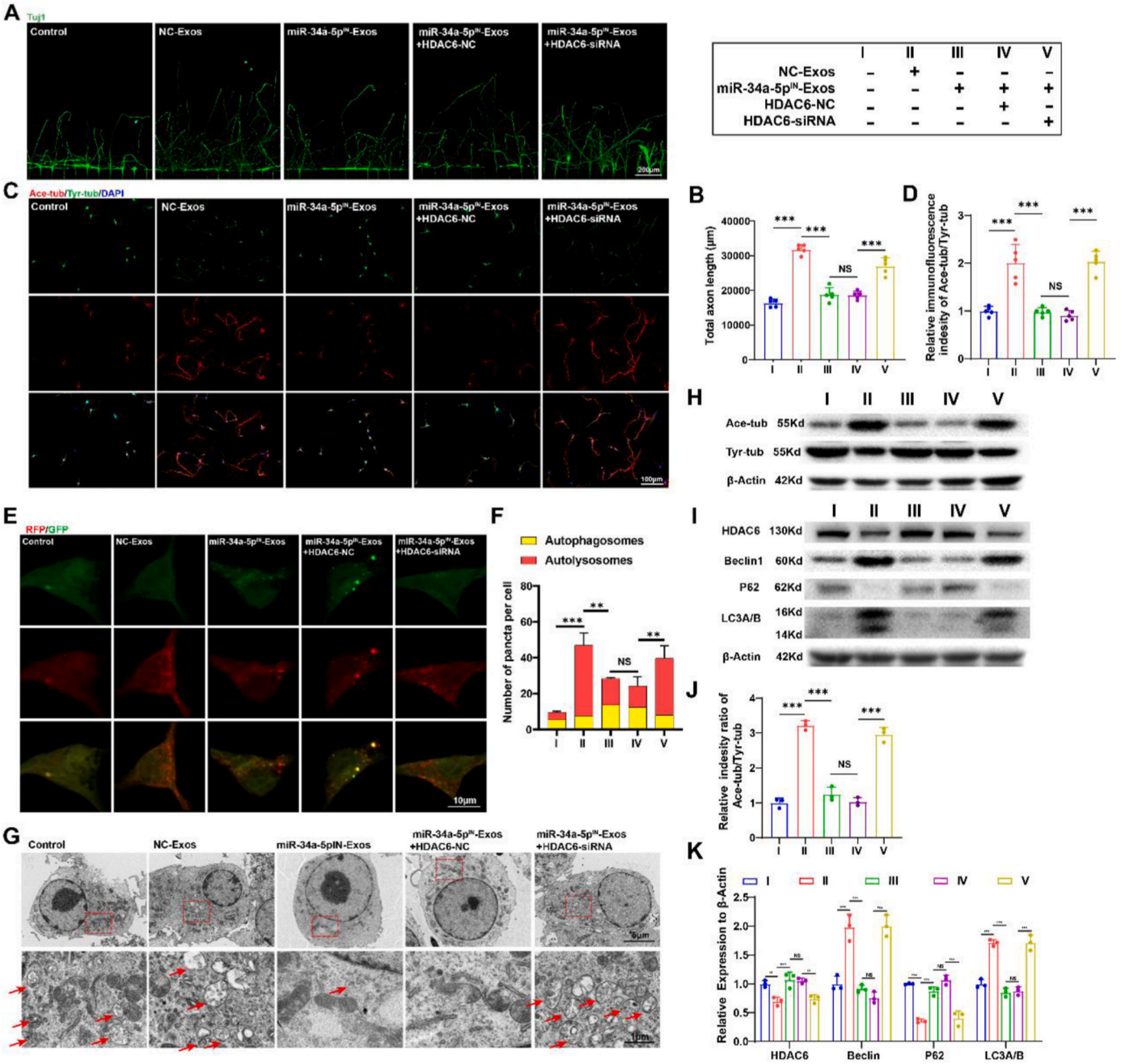

Fig. 8. EGFR $^{+}$ NSCs-Exos stabilized the microtubules and activated autophagy via the miR-34a-5p/HDAC6 pathway.
(A) Representative immunofluorescent images of the regenerative axons on the microfluidic culture plate (green: Tuj1) of the control, NC-Exos, miR-34a-5p^{IN}-Exos, miR-34a-5p^{IN}-Exos + HDAC6-NC, and miR-34a-5p^{IN}-Exos + HDAC6 siRNA group. (B) Quantification of total axonal length in (A). N = 5 per group. (C) Representative immunofluorescence staining of Ace-tub and Tyr-tub images within the cultured neurons. (D) Quantification of the relative expression of Ace-tub/Tyr-tub ratio in (C). N = 5 per group. (E) Autophagy flux in cultured neurons visualized by mRFP-GFP-LC3. Yellow and red puncta respectively represent autophagosomes and autolysosomes. (F) Quantification of autophagosomes and autolysosomes counts in (E), N = 5 per group. (G) Electron microscope images of cultured neurons in vitro (scale bar, 5 μm) and higher magnification of the dotted-line squares in the upper images (scale bar, 1 μm). The red arrows indicated the autophagosomes. (H) Western blot analysis of Ace-tub and Tyr-tub expression in cultured neurons. (I) Western blot analysis of autophagy relative proteins HDAC6, LC3A/B, Beclin1, and P62 expression in cultured neurons. (J) Quantification of relative Ace-tub/Tyr-tub ratio in (H). N = 3 per group. (K) Quantification of LC3A/B, Beclin1, and P62 expression in (I). N = 3 per group. Data are presented as mean ± SD; NS, no significant difference; *$P < 0.05$, **$P < 0.01$, and ***$P < 0.001$.

revealed decreased GAP43 and NF-positive signaling in the spinal cord of the miR-34a-5p^{IN}-Exos treated mice. The administration of SW-100 could rescue the inhibition effects of miR-34a-5p^{IN}-Exos on promoting intrinsic neurite growth (Fig. 9G–J). The in vitro neural regrowth assay was also conducted and found similar effects as the in vivo data (Fig. 9E–F and Figs. S10E–F). These results indicated that EGFR^{+}N-SC-Exos promoted functional recovery post-SCI via the miR-34a-5p/HDAC6 pathway.

4. Discussion

In our current study, we identified a subtype of NSCs, named EGFR^{+}NSCs, and extracted their secreted exosomes, which were superior to primary NSCs derived exosomes in aiding SCI repair. In the

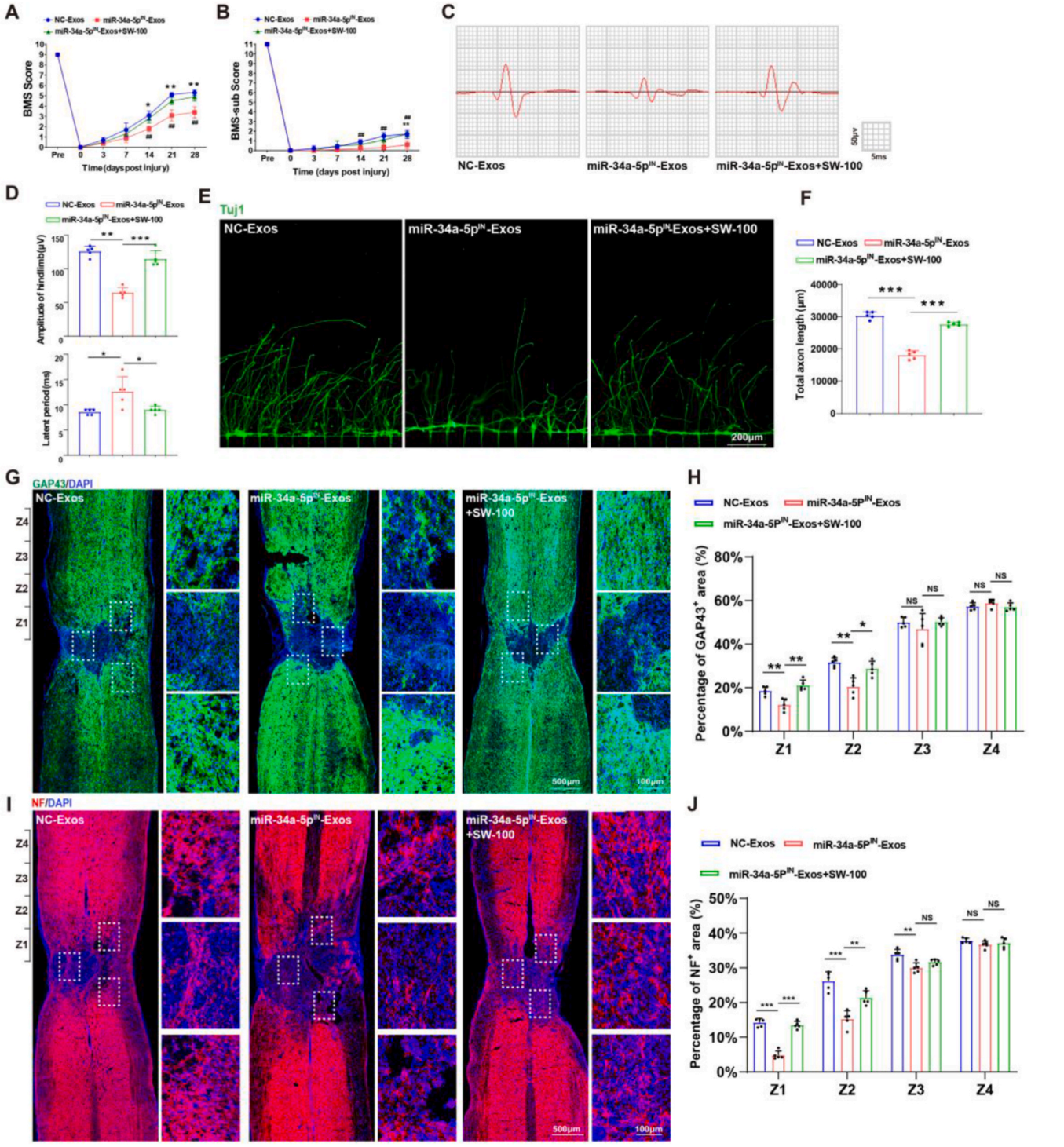

Fig. 9. EGFR $^{+}$ NSC-Exos promoted functional recovery post-SCI via miR-34a-5p/HDAC6 pathway

(A) BMS scores in NC-Exos, miR-34a-5p^{IN}-Exos, and miR-34a-5p^{IN}-Exos + SW100, groups at different time points post-SCI. N = 5 per group. * miR-34a-5p^{IN}-Exos vs miR-34a-5p^{IN}-Exos + SW100 , # NC-Exos vs miR-34a-5p^{IN}-Exos. (B) BMS sub scores in NC-Exos, miR-34a-5p^{IN}-Exos, and miR-34a-5p^{IN}-Exos + SW100 groups at different time points post-SCI. N = 5 per group. (C) Representative electrophysiological trace images were recorded in each group at 28 days post-SCI. (D) Measurement of the MEPs, amplitude, and latent period in (C). N = 5 per group. (E) Representative immunofluorescent images of the regenerative axons on the microfluidic culture plate (green: Tuj1). (F) Quantification of total axonal length in (E). N = 5 per group. (G) Representative immunofluorescent stains of GAP43 images of the spinal cord at 28 days post-injury in each group. The Z1-Z4 indicates the area sequential 500 μm roster to the epicenter. Scale bar, 500 μm. (H) Quantification of GAP43 positive signals in different areas roster to the epicenter of NC-Exos, miR-34a-5p^{IN}-Exos, and miR-34a-5p^{IN}-Exos + SW100 groups in (G). N = 5 per group. (I) Representative immunofluorescent stains of NF images of the spinal cord at 28 days post-injury in each group. The Z1-Z4 indicates the area sequential 500 μm roster to the epicenter. Scale bar, 500 μm. (J) Quantification of NF positive signals in different areas roster to the epicenter of NC-Exos, miR-34a-5p^{IN}-Exos, and miR-34a-5p^{IN}-Exos + SW100 groups in (I). N = 5 per group. Data are presented as mean ± SD, NS, no significant difference; $*/^{\#}P < 0.05$, $**/^{\#\#}P < 0.01$, $***/^{\#\#\#}P < 0.001$.

meantime, we generated a 3D-printed hydrogel patch loading with EGFR$^+$NSCs-Exos, and demonstrated that it can be sustained by releasing exosomes, which could cross the blood-spinal cord barrier and downregulate HDAC6 in neurons by locally delivering exosomal miR-34a-5p. Inhibiting HDAC6 by miR-34a-5p activated the autophagy pathway and promoted microtubule stability to facilitate neurite growth and neurological functional recovery after SCI. It highlights that the local delivery of EGFR$^+$NSCs-derived exosomes can serve as a novel therapeutic agent for spinal cord injury repair.

Previous studies have shown that SCI can lead to severe disruption of neural networks and loss of neurological function. Due to their ability to self-renew and differentiate into different cell types, NSCs hold great promise in cell replacement therapy for SCI. Transplanted neural stem cells exert their neuroprotective effects by promoting neurite outgrowth [28,50]. However, in terms of clinical application and ethical issues, direct transplantation of NSCs is highly controversial and raises safety concerns [31,32]. As a novel "cell-free" therapy, stem cell-derived exosomes have attracted therapeutic attention due to their unique biological properties [51]. Our previous research demonstrated for the first time that the primary NSCs-derived exosomes have a neuroprotective effect for promoting SCI repair by enhancing angiogenesis [2]. In our subsequent investigations, we have explored a specific subtype of immune cell-derived exosomes, which may contribute to enhancing the efficiency and quality of exosome-based therapies. The results demonstrated that exosomes derived from M2 macrophage could deliver OTULIN to vascular endothelial cells in the injured spinal cord, and promote vascular regeneration through activation of the Wnt/β-catenin pathway [8].

Adult NSCs in the mammalian central nervous system are characterized by maintaining an undifferentiated and quiescent state (qNSCs), and occasionally transitioning from a quiescent state into an active state to generate new neurons [24]. Upon activation, qNSCs upregulate EGFR and become highly proliferative. Single-cell RNA-sequencing analysis revealed that there are two distinct subsets of NSCs, named quiescent and active NSCs, with distinct molecular and functional properties. Active NSCs (aNSCs) were enriched in genes involved in transcription, translation and DNA repair, while quiescent cells were enriched in transcripts associated with cell adhesion and extracellular matrix [25]. Notably, neurogenic transcription factors such as Dlx 1, Dlx 2, Sox 4 and Ascl1, which are hallmarks of NSCs, are predominantly expressed in aNSCs. qNSCs produced few neurospheres and did not increase their neurosphere formation efficiency during regeneration. In contrast, aNSCs extensively formed neurospheres and adherent colonies [26]. These results suggest that the biological functional properties of aNSCs may be stronger than that of qNSCs. In our research, we performed a series of experiments to validate that a subtype of NSCs, EGFR-positive NSCs-derived exosomes have a better therapeutic effect than primary NSCs exosomes in SCI repair. We found that EGFR$^+$NSC derived exosomes could be taken up by neurons in the injured area after SCI, and significantly promote the growth of neurites after spinal cord injury, suggesting that EGFR$^+$NSC derived exosomes may play a role in neurite growth by affecting neurogenesis-related-pathways in neurons.

Exosomes can transfer a variety of biologically active components (miRNAs, mRNAs, DNAs, proteins, etc.) to recipient cells, among which, exosome-loaded miRNAs are the most critical cargo mediating biological functions [33]. miRNAs are small non-coding regulatory RNAs that bind to the complementary sequence of the 3-untranslated region (3′UTR) of target mRNAs and can inhibit translation or lead to degradation of target mRNAs [40]. In this study, we screened the highly expressed miRNA components in exosomes derived from EGFR$^+$ NSCs using miRNA-seq. We found that miR-34a-5p was highly expressed in EGFR$^+$NSCs-derived exosomes, and could mediate the effect of EGFR$^+$NSCs-derived exosomes for promoting neurite regeneration. miR-34 has been identified as a key regulator of neural differentiation and proliferation. Pandey et al. found that the miR-34 family was one of the most significantly elevated miRNAs during neural differentiation of PC12 cells treated with nerve growth factor (NGF) [52]. Jauhari et al. discovered that miR-34a-5p could target p53, protecting cells from p53-induced death [53]. Aranha et al. confirmed that miR-34a could control the differentiation of NSCs. Overexpression of miR-34a-5p resulted in increased neurite extension in differentiated neurons of NSCs, whereas decreased expression of miR-34a prevented neuronal differentiation [54]. Another research showed that miR-34a affected Notch signaling, possibly by targeting the Notch ligand Dll 1, which controlled neuronal differentiation and cell growth [55]. However, there is no relevant literature on the application of exosomal miR-34a-5p in SCI management. To clarify the role of miR-34a-5p in EGFR$^+$NSCs-derived exosomes, we used the inhibitor of miR-34a-5p to intervene in the expression of miR-34a-5p in the obtained EGFR$^+$NSCs derived exosomes. We found that the positive effect of EGFR$^+$NSCs derived exosomes on SCI treatment was attenuated after reducing the expression of miR-34a-5p in exosomes, suggesting that miR-34a-5p was a key component in EGFR$^+$NSCs derived exosomes for promoting neurite growth after SCI. Considering that exosomes carry a variety of biologically active molecules, culturing NSCs with miR-34a-5p inhibitor may lead to the accumulation of other bioactive factors in the derived exosomes. Therefore, whether EGFR$^+$NSCs derived exosomes promote SCI repair through other factors remains to be further investigated.

The integrity of the spinal cord parenchyma, including axon connectivity, is disrupted immediately after trauma. Due to the limited neuroplasticity, impaired axons are hard to grow across the lesion [56]. Therefore, any therapeutic strategy aimed at promoting neuroplasticity, neurogenesis, and reconstruction of damaged neural circuits is necessary to improve neurological healing after SCI. Neurons utilize microtubules as their main structural element to produce elongated axons. Acetylation, which plays a crucial role in the stability of microtubules, primarily takes place in the luminal region of microtubules at the Lys 40 residue of α-tubulin. This process modifies the interaction between protofibrils, increasing stiffness and protecting them from damage caused by mechanical stress [57,58]. The maturation of microtubules requires detyrosinylation. Tyrosinated α-tubulin is indicative of the formation of nascent microtubules and reflects the dynamics of microtubules. Promoting the expression of tyrosinated tubulin can lead to microtubule destabilization. Therefore, the ratio of acetylated to tyrosinated α-tubulin (A/T ratio) was used as a reliable method for quantitatively comparing microtubule stability properties [59,60]. And the non-histone protein acetylation influences a myriad of cellular and physiological processes, including transcription, autophagy, mitosis, differentiation and neural function [61], in which neural autophagy plays a beneficial role of autophagy in axon regeneration [62]. Therefore, targeting the microtubule stability after neural damage may be a potential target for spinal cord injury treatment. HDACs are proteases that regulate chromosomal structure and the expression of various genes. Among HDACs, HDAC6 is the only HDAC located in the cytoplasm, which regulates the deacetylation of non-histone structures or substrates and is involved in various physiological and pathological processes such as microtubule stabilization and autophagy [48]. HDAC6 has been reported to promote neurite growth by inhibiting the level of autophagy and affecting the acetylation level of neural microtubules, thereby improving the stability of microtubules [57,58]. In the present study, we found that EGFR$^+$NSCs derived exosomal miR-34a-5p could regulate the expression of HDAC6 to increase the acetylation level of neurite microtubules, while decreasing the level of tyrosination of neurite microtubules, and finally promote the extension of neurites.

After adult SCI, insufficient axon regeneration will lead to poor recovery, which is the most urgent problem to be solved in the treatment of SCI. Unlike neurite outgrowth during development, adult axon regeneration is characterized by insufficient intrinsic neuronal growth capability, lack of adequate neurotrophic factor support, and lack of guidance from the nerve growth matrix [63]. Previous studies suggested that NSC-derived exosomes promoted angiogenesis through the delivery of VEGF, and these remodeled vessels could provide scaffolds for neurite

extension [2]. NSC-derived exosomes could alleviate neuroinflammation to promote the production and accumulation of neurotrophic factors, thus providing a favorable microenvironment for the extension of neurites [38,64]. In the present study, we explored the effect of EGFR$^+$NSCs derived exosomes and demonstrated it could trigger the intrinsic neurite outgrowth ability of neurons. In addition, we also found that EGFR$^+$NSCs-Exos could internalized by the phagocytes and other tissue cells (astrocytes, endothelial cells, etc.). However, whether EGFR$^+$NSCs derived exosomes could improve functional recovery after SCI through other mechanisms, needs to be further explored.

Systemically delivered exosomes (Intravenous, Oral administration, Intraperitoneal injection, etc.) may cause exosome accumulation at the non-injured sites or rapidly eliminated from the body through fluids [44]. Direct injection of exosomes could rapidly clear and caused secondary injuries to the spinal cord [65]. These approaches limit their therapeutic effects. The impact of GelMA-based hydrogels is emerging as a promising material on the preclinical SCI landscape due to their advantageous properties such as plasticity, biocompatibility, and biodegradability [10,66,67]. To overcome rapid clearance and sustain exosome bioactivity, we encapsulated these small vesicles in GelMA hydrogels to achieve protection and sustained release. We characterized the physicochemical properties of this GelMA-based hydrogel and confirmed that this exosomes-hydrogel control release system possesses excellent biocompatibility and gradual degradation. Our 3D-printed tissue-engineered patches with high plasticity enable local and sustained delivery of exosomes in the injured site of the spinal cord after SCI with long-term maintenance, which can minimize the problems caused by the rapid administration of exosomes with the above-mentioned methods, and provides us with novel prospects for the treatment of spinal cord injury.

In conclusion, this study demonstrates that local administration of 3D-printed hydrogel patch coated EGFR$^+$NSCs-Exos could transfer miR-34a-5p into neurons to inhibit the expression of HDAC6. Reduction of HDAC6 increased the stability of microtubules and activated autophagy, which in turn promoted neurite regrowth in the injury site of the spinal cord after SCI and improved their neurological function recovery. Our research provided a novel and precise cell-free therapeutic strategy for SCI repair.

Data availability

The data that support the findings of this study are available from the corresponding author upon reasonable request.

Ethics approval and consent to participate

The experimental design followed the “3 R” principle. Animals were maintained in standard, specific pathogen-free (SPF) conditions of the Department of Laboratory Animals, Central South University (CSU) with 12 light/12 dark cycles and 4–5 mice per cage. All mice in this study were kept on a standard normal chow diet. All animal experiments were approved by the Ethics Committee of CSU for Scientific Research. All the authors listed consented with all relevant ethical regulations.

CRediT authorship contribution statement

Tian Qin: Writing – review & editing, Writing – original draft, Data curation. **Chengjun Li:** Writing – review & editing, Writing – original draft, Formal analysis. **Yan Xu:** Methodology. **Yiming Qin:** Software, Methodology. **Yuxin Jin:** Methodology. **Rundong He:** Methodology. **Zixiang Luo:** Methodology. **Jinyun Zhao:** Methodology. **Chunyue Duan:** Investigation, Funding acquisition. **Hongbin Lu:** Writing – review & editing, Funding acquisition. **Yong Cao:** Writing – review & editing, Funding acquisition. **Jianzhong Hu:** Writing – review & editing, Validation, Investigation, Funding acquisition.

Declaration of competing interest

The authors have no conflicts of interest relevant to this article.

Acknowledgments

This work was funded by the National Natural Science Foundation of China (grant 82030071, 82272495), and the Science and Technology Major Project of Changsha, China (NO. kh2103008).

Appendix A. Supplementary data

Supplementary data to this article can be found online at https://doi.org/10.1016/j.bioactmat.2023.11.013.

References

[1] M. Li, Z.-J. Rong, Y. Cao, L.-Y. Jiang, D. Zhong, C.-J. Li, X.-L. Sheng, J.-Z. Hu, H.-B. Lu, Regulates the NF-κB signaling pathway of natural stem cells to modulate macrophage migration during spinal cord injury, J. Neurotrauma 38 (2021) 353–364, https://doi.org/10.1089/neu.2020.7075.

[2] D. Zhong, Y. Cao, C.-J. Li, M. Li, Z.-J. Rong, L. Jiang, Z. Guo, H.-B. Lu, J.-Z. Hu, Neural stem cell-derived exosomes facilitate spinal cord functional recovery after injury by promoting angiogenesis, Exp. Biol. Med. 245 (2020) 54–65, https://doi.org/10.1177/1535370219895491.

[3] Z. Guo, C. Li, Y. Cao, T. Qin, L. Jiang, Y. Xu, M. Li, Z. Luo, J. Hu, H. Lu, UTX/KDM6A deletion promotes the recovery of spinal cord injury by epigenetically triggering intrinsic neural regeneration, Mol Ther Methods Clin Dev 20 (2021) 337–349, https://doi.org/10.1016/j.omtm.2020.12.004.

[4] H.J. Kim, J. Magrané, Isolation and culture of neurons and astrocytes from the mouse brain cortex, Methods Mol. Biol. 793 (2011) 63–75, https://doi.org/10.1007/978-1-61779-328-8_4.

[5] J.W. Park, B. Vahidi, A.M. Taylor, S.W. Rhee, N.L. Jeon, Microfluidic culture platform for neuroscience research, Nat. Protoc. 1 (2006) 2128–2136.

[6] R. Xu, A. Yallowitz, A. Qin, Z. Wu, D.Y. Shin, J.-M. Kim, S. Debnath, G. Ji, M. P. Bostrom, X. Yang, C. Zhang, H. Dong, P. Kermani, S. Lalani, N. Li, Y. Liu, M. G. Poulos, A. Wach, Y. Zhang, K. Inoue, A. Di Lorenzo, B. Zhao, J.M. Butler, J.-H. Shim, L.H. Glimcher, M.B. Greenblatt, Targeting skeletal endothelium to ameliorate bone loss, Nat. Med. 24 (2018) 823–833, https://doi.org/10.1038/s41591-018-0020-z.

[7] C.-Y. Chen, S.-S. Rao, L. Ren, X.-K. Hu, Y.-J. Tan, Y. Hu, J. Luo, Y.-W. Liu, H. Yin, J. Huang, J. Cao, Z.-X. Wang, Z.-Z. Liu, H.-M. Liu, S.-Y. Tang, R. Xu, H. Xie, Exosomal DMBT1 from human urine-derived stem cells facilitates diabetic wound repair by promoting angiogenesis, Theranostics 8 (2018) 1607–1623, https://doi.org/10.7150/thno.22958.

[8] Z. Luo, W. Peng, Y. Xu, Y. Xie, Y. Liu, H. Lu, Y. Cao, J. Hu, Exosomal OTULIN from M2 macrophages promotes the recovery of spinal cord injuries via stimulating Wnt/β-catenin pathway-mediated vascular regeneration, Acta Biomater. 136 (2021) 519–532, https://doi.org/10.1016/j.actbio.2021.09.026.

[9] X. Ge, H. Wen, Y. Fei, R. Xue, Z. Cheng, Y. Li, K. Cai, L. Li, M. Li, Z. Luo, Structurally dynamic self-healable hydrogel cooperatively inhibits intestinal inflammation and promotes mucosal repair for enhanced ulcerative colitis treatment, Biomaterials 299 (2023), 122184, https://doi.org/10.1016/j.biomaterials.2023.122184.

[10] C.M. Walsh, J.K. Wychowaniec, L. Costello, D.F. Brougham, D. Dooley, An in vitro and ex vivo analysis of the potential of GelMA hydrogels as a therapeutic platform for preclinical spinal cord injury, Adv. Healthcare Mater. (2023), e2300951, https://doi.org/10.1002/adhm.202300951.

[11] L. Fan, C. Liu, X. Chen, L. Zheng, Y. Zou, H. Wen, P. Guan, F. Lu, Y. Luo, G. Tan, P. Yu, D. Chen, C. Deng, Y. Sun, L. Zhou, C. Ning, Exosomes-loaded electroconductive hydrogel synergistically Pro0bvvmotes tissue repair after spinal cord injury via immunoregulation and enhancement of myelinated axon growth, Adv. Sci. 9 (2022), e2105586, https://doi.org/10.1002/advs.202105586.

[12] H. Hu, L. Dong, Z. Bu, Y. Shen, J. Luo, H. Zhang, S. Zhao, F. Lv, Z. Liu, miR-23a-3p-abundant small extracellular vesicles released from Gelma/nanoclay hydrogel for cartilage regeneration, J. Extracell. Vesicles 9 (2020), 1778883, https://doi.org/10.1080/20013078.2020.1778883.

[13] S. Ni, Z. Luo, L. Jiang, Z. Guo, P. Li, X. Xu, Y. Cao, C. Duan, T. Wu, C. Li, H. Lu, J. Hu, UTX/KDM6A deletion promotes recovery of spinal cord injury by epigenetically regulating vascular regeneration, Mol. Ther. : the journal of the American Society of Gene Therapy 27 (2019) 2134–2146, https://doi.org/10.1016/j.ymthe.2019.08.009.

[14] D.M. Basso, L.C. Fisher, A.J. Anderson, L.B. Jakeman, D.M. McTigue, P. G. Popovich, Basso Mouse Scale for locomotion detects differences in recovery after spinal cord injury in five common mouse strains, J. Neurotrauma 23 (2006) 635–659.

[15] C. Li, T. Qin, Y. Liu, H. Wen, J. Zhao, Z. Luo, W. Peng, H. Lu, C. Duan, Y. Cao, J. Hu, Microglia-derived exosomal microRNA-151-3p enhances functional healing after spinal cord injury by attenuating neuronal apoptosis regulating the p53/p21/CDK1 signaling pathway, Front. Cell Dev. Biol. 9 (2021), 783017, https://doi.org/10.3389/fcell.2021.783017.

[16] P. Hundeshagen, A. Hamacher-Brady, R. Eils, N.R. Brady, Concurrent detection of autolysosome formation and lysosomal degradation by flow cytometry in a high-content screen for inducers of autophagy, BMC Biol. 9 (2011) 38, https://doi.org/10.1186/1741-7007-9-38.
[17] J.W. McDonald, C. Sadowsky, Spinal-cord injury, Lancet 359 (2002) 417–425.
[18] GBD 2016 Traumatic Brain Injury and Spinal Cord Injury Collaborators, National burden of traumatic brain injury and spinal cord injury, 1990-2016: a systematic analysis for the Global Burden of Disease Study 2016, Lancet Neurol. 18 (2019) 56–87, https://doi.org/10.1016/S1474-4422(18)30415-0.
[19] B. Li, J. Qi, P. Cheng, P. Yin, G. Hu, L. Wang, Y. Liu, J. Liu, X. Zeng, J. Hu, M. Zhou, Traumatic spinal cord injury mortality from 2006 to 2016 in China, The journal of spinal cord medicine 44 (2021) 1005–1010, https://doi.org/10.1080/10790268.2019.1699355.
[20] Spinal cord injury (SCI) 2016 facts and figures at a glance, The journal of spinal cord medicine 39 (2016) 493–494, https://doi.org/10.1080/10790268.2016.1210925.
[21] N.A. Silva, N. Sousa, R.L. Reis, A.J. Salgado, From basics to clinical: a comprehensive review on spinal cord injury, Prog. Neurobiol. 114 (2014) 25–57, https://doi.org/10.1016/j.pneurobio.2013.11.002.
[22] T.H. Hutson, S. Di Giovanni, The translational landscape in spinal cord injury: focus on neuroplasticity and regeneration, Nat. Rev. Neurol. 15 (2019) 732–745, https://doi.org/10.1038/s41582-019-0280-3.
[23] M. Götz, S. Sirko, J. Beckers, M. Irmler, Reactive astrocytes as neural stem or progenitor cells: in vivo lineage, in vitro potential, and Genome-wide expression analysis, Glia 63 (2015) 1452–1468, https://doi.org/10.1002/glia.22850.
[24] G. Belenguer, P. Duart-Abadia, A. Jordán-Pla, A. Domingo-Muelas, L. Blasco-Chamarro, S.R. Ferrón, J.M. Morante-Redolat, I. Fariñas, Adult neural stem cells are alerted by systemic inflammation through TNF-α receptor signaling, Cell Stem Cell 28 (2021), https://doi.org/10.1016/j.stem.2020.10.016.
[25] E. Llorens-Bobadilla, S. Zhao, A. Baser, G. Saiz-Castro, K. Zwadlo, A. Martin-Villalba, Single-cell transcriptomics reveals a population of dormant neural stem cells that become activated upon brain injury, Cell Stem Cell 17 (2015) 329–340, https://doi.org/10.1016/j.stem.2015.07.002.
[26] G. Kalamakis, D. Brune, S. Ravichandran, J. Bolz, W. Fan, F. Ziebell, T. Stiehl, F. Catala-Martinez, J. Kupke, S. Zhao, E. Llorens-Bobadilla, K. Bauer, S. Limpert, B. Berger, U. Christen, P. Schmezer, J.P. Mallm, B. Berninger, S. Anders, A. Del Sol, A. Marciniak-Czochra, A. Martin-Villalba, Quiescence modulates stem cell maintenance and regenerative capacity in the aging brain, Cell 176 (2019) 1407–1419 e1414, https://doi.org/10.1016/j.cell.2019.01.040.
[27] E. Curtis, J.R. Martin, B. Gabel, N. Sidhu, T.K. Rzesiewicz, R. Mandeville, S. Van Gorp, M. Leerink, T. Tadokoro, S. Marsala, C. Jamieson, M. Marsala, J.D. Ciacci, A first-in-human, phase I study of neural stem cell transplantation for chronic spinal cord injury, Cell Stem Cell 22 (2018), https://doi.org/10.1016/j.stem.2018.05.014.
[28] S. Ceto, K.J. Sekiguchi, Y. Takashima, A. Nimmerjahn, M.H. Tuszynski, Neural stem cell grafts form extensive synaptic networks that integrate with host circuits after spinal cord injury, Cell Stem Cell 27 (2020), https://doi.org/10.1016/j.stem.2020.07.007.
[29] A. Tsukamoto, N. Uchida, A. Capela, T. Gorba, S. Huhn, Clinical translation of human neural stem cells, Stem Cell Res. Ther. 4 (2013) 102, https://doi.org/10.1186/scrt313.
[30] F. Li, J. Zhang, A. Chen, R. Liao, Y. Duan, Y. Xu, L. Tao, Combined transplantation of neural stem cells and bone marrow mesenchymal stem cells promotes neuronal cell survival to alleviate brain damage after cardiac arrest microRNA-133b incorporated in extracellular vesicles, Aging (Albany NY) 13 (2021) 262–278, https://doi.org/10.18632/aging.103920.
[31] S. Pluchino, J.A. Smith, L. Peruzzotti-Jametti, Promises and limitations of neural stem cell therapies for progressive multiple sclerosis, Trends Mol. Med. 26 (2020) 898–912, https://doi.org/10.1016/j.molmed.2020.04.005.
[32] A.S. Lee, C. Tang, M.S. Rao, I.L. Weissman, J.C. Wu, Tumorigenicity as a clinical hurdle for pluripotent stem cell therapies, Nat. Med. 19 (2013), https://doi.org/10.1038/nm.3267.
[33] R. Kalluri, V.S. LeBleu, The Biology Function and Biomedical Applications of Exosomes, Science, New York, N.Y., 2020, p. 367, https://doi.org/10.1126/science.aau6977.
[34] C. Li, T. Qin, J. Zhao, R. He, H. Wen, C. Duan, H. Lu, Y. Cao, J. Hu, Bone marrow mesenchymal stem cell-derived exosome-educated macrophages promote functional healing after spinal cord injury, Front. Cell. Neurosci. 15 (2021), https://doi.org/10.3389/fncel.2021.725573.
[35] X. Sheng, J. Zhao, M. Li, Y. Xu, Y. Zhou, J. Xu, R. He, H. Lu, T. Wu, C. Duan, Y. Cao, J. Hu, Bone marrow mesenchymal stem cell-derived exosomes accelerate functional recovery after spinal cord injury by promoting the phagocytosis of macrophages to clean myelin debris, Front. Cell Dev. Biol. 9 (2021), 772205, https://doi.org/10.3389/fcell.2021.772205.
[36] G. Belenguer, P. Duart-Abadia, A. Jordán-Pla, A. Domingo-Muelas, L. Blasco-Chamarro, S.R. Ferrón, J.M. Morante-Redolat, I. Fariñas, Adult neural stem cells are alerted by systemic inflammation through TNF-α receptor signaling, Cell Stem Cell 28 (2021) 285–299.e289, https://doi.org/10.1016/j.stem.2020.10.016.
[37] R.L. Webb, E.E. Kaiser, S.L. Scoville, T.A. Thompson, S. Fatima, C. Pandya, K. Sriram, R.L. Swetenburg, K. Vaibhav, A.S. Arbab, B. Baban, K.M. Dhandapani, D. C. Hess, M.N. Hoda, S.L. Stice, Human neural stem cell extracellular vesicles improve tissue and functional recovery in the murine thromboembolic stroke model, Translational stroke research 9 (2018) 530–539, https://doi.org/10.1007/s12975-017-0599-2.
[38] Y. Rong, W. Liu, J. Wang, J. Fan, Y. Luo, L. Li, F. Kong, J. Chen, P. Tang, W. Cai, Neural stem cell-derived small extracellular vesicles attenuate apoptosis and neuroinflammation after traumatic spinal cord injury by activating autophagy, Cell Death Dis. 10 (2019) 340, https://doi.org/10.1038/s41419-019-1571-8.
[39] Y. Rong, W. Liu, C. Lv, J. Wang, Y. Luo, D. Jiang, L. Li, Z. Zhou, W. Zhou, Q. Li, G. Yin, L. Yu, J. Fan, W. Cai, Neural stem cell small extracellular vesicle-based delivery of 14-3-3t reduces apoptosis and neuroinflammation following traumatic spinal cord injury by enhancing autophagy by targeting Beclin-1, Aging (Albany NY) 11 (2019) 7723–7745, https://doi.org/10.18632/aging.102283.
[40] Y.S. Lee, A. Dutta, MicroRNAs in cancer, Annu. Rev. Pathol. 4 (2009) 199–227, https://doi.org/10.1146/annurev.pathol.4.110807.092222.
[41] C. Ma, P. Zhang, Y. Shen, Progress in research into spinal cord injury repair: tissue engineering scaffolds and cell transdifferentiation, J. Neurorestoratol. 7 (2019) 196–206, https://doi.org/10.26599/JNR.2019.9040024.
[42] R. Deng, Z. Luo, Z. Rao, Z. Lin, S. Chen, J. Zhou, Q. Zhu, X. Liu, Y. Bai, D. Quan, Decellularized extracellular matrix containing electrospun fibers for nerve regeneration: a comparison between core–shell structured and preblended composites, Advanced Fiber Materials 4 (2022) 503–519, https://doi.org/10.1007/s42765-021-00124-5.
[43] S. Kabu, Y. Gao, B.K. Kwon, V. Labhasetwar, Drug delivery, cell-based therapies, and tissue engineering approaches for spinal cord injury, J. Contr. Release 219 (2015) 141–154, https://doi.org/10.1016/j.jconrel.2015.08.060.
[44] L. Barile, G. Vassalli, Exosomes: therapy delivery tools and biomarkers of diseases, Pharmacology & Therapeutics 174 (2017) 63–78, https://doi.org/10.1016/j.pharmthera.2017.02.020.
[45] B. Lv, L. Lu, L. Hu, P. Cheng, Y. Hu, X. Xie, G. Dai, B. Mi, X. Liu, G. Liu, Recent advances in GelMA hydrogel transplantation for musculoskeletal disorders and related disease treatment, Theranostics 13 (2023) 2015–2039, https://doi.org/10.7150/thno.80615.
[46] X. Li, H. Saiyin, X. Chen, Q. Yu, L. Ma, W. Liang, Ketamine impairs growth cone and synaptogenesis in human GABAergic projection neurons via GSK-3β and HDAC6 signaling, Mol. Psychiatr. (2022), https://doi.org/10.1038/s41380-022-01864-5.
[47] A.R. Esteves, A.M. Palma, R. Gomes, D. Santos, D.F. Silva, S.M. Cardoso, Acetylation as a major determinant to microtubule-dependent autophagy: relevance to Alzheimer's and Parkinson disease pathology, Biochim. Biophys. Acta, Mol. Basis Dis. 1865 (2019) 2008–2023, https://doi.org/10.1016/j.bbadis.2018.11.014.
[48] C. Hubbert, A. Guardiola, R. Shao, Y. Kawaguchi, A. Ito, A. Nixon, M. Yoshida, X.-F. Wang, T.-P. Yao, HDAC6 is a microtubule-associated deacetylase, Nature 417 (2002) 455–458.
[49] A.P. Kozikowski, S. Shen, M. Pardo, M.T. Tavares, D. Szarics, V. Benoy, C. A. Zimprich, Z. Kutil, G. Zhang, C. Bařinka, M.B. Robers, L. Van Den Bosch, J. H. Eubanks, R.S. Jope, Brain penetrable histone deacetylase 6 inhibitor SW-100 ameliorates memory and learning impairments in a mouse model of fragile X syndrome, ACS Chem. Neurosci. 10 (2019) 1679–1695, https://doi.org/10.1021/acschemneuro.8b00600.
[50] J.F. Bonner, T.M. Connors, W.F. Silverman, D.P. Kowalski, M.A. Lemay, I. Fischer, Grafted neural progenitors integrate and restore synaptic connectivity across the injured spinal cord, J. Neurosci. : the official journal of the Society for Neuroscience 31 (2011) 4675–4686, https://doi.org/10.1523/JNEUROSCI.4130-10.2011.
[51] D. Dutta, N. Khan, J. Wu, S.M. Jay, Extracellular vesicles as an emerging frontier in spinal cord injury pathobiology and therapy, Trends Neurosci. 44 (2021) 492–506, https://doi.org/10.1016/j.tins.2021.01.003.
[52] D. Aberdam, E. Candi, R.A. Knight, G. Melino, miRNAs, 'stemness' and skin, Trends Biochem. Sci. 33 (2008) 583–591, https://doi.org/10.1016/j.tibs.2008.09.002.
[53] A. Jauhari, T. Singh, P. Singh, D. Parmar, S. Yadav, Regulation of miR-34 family in neuronal development, Mol. Neurobiol. 55 (2018) 936–945, https://doi.org/10.1007/s12035-016-0359-4.
[54] M.M. Aranha, D.M. Santos, S. Solá, C.J. Steer, C.M.P. Rodrigues, miR-34a regulates mouse neural stem cell differentiation, PLoS One 6 (2011), e21396, https://doi.org/10.1371/journal.pone.0021396.
[55] P. de Antonellis, C. Medaglia, E. Cusanelli, I. Andolfo, L. Liguori, G. De Vita, M. Carotenuto, A. Bello, F. Formiggini, A. Galeone, G. De Rosa, A. Virgilio, I. Scognamiglio, M. Sciro, G. Basso, J.H. Schulte, G. Cinalli, A. Iolascon, M. Zollo, MiR-34a targeting of Notch ligand delta-like 1 impairs CD15+/CD133+ tumor-propagating cells and supports neural differentiation in medulloblastoma, PLoS One 6 (2011), e24584, https://doi.org/10.1371/journal.pone.0024584.
[56] C.S. Ahuja, J.R. Wilson, S. Nori, M.R.N. Kotter, C. Druschel, A. Curt, M.G. Fehlings, Traumatic spinal cord injury, Nat. Rev. Dis. Prim. 3 (2017), 17018, https://doi.org/10.1038/nrdp.2017.18.
[57] A.L. Kalinski, A.N. Kar, J. Craver, A.P. Tosolini, J.N. Sleigh, S.J. Lee, A. Hawthorne, P. Brito-Vargas, S. Miller-Randolph, R. Passino, L. Shi, V.S.C. Wong, C. Picci, D. S. Smith, D.E. Willis, L.A. Havton, G. Schiavo, R.J. Giger, B. Langley, J.L. Twiss, Deacetylation of Miro 1 by HDAC6 blocks mitochondrial transport and mediates axon growth inhibition, J. Cell Biol. 218 (2019) 1871–1890, https://doi.org/10.1083/jcb.201702187.
[58] K.A. Han, W.H. Shin, S. Jung, W. Seol, H. Seo, C. Ko, K.C. Chung, Leucine-rich repeat kinase 2 exacerbates neuronal cytotoxicity through phosphorylation of histone deacetylase 3 and histone deacetylation, Hum. Mol. Genet. (2017) 26, https://doi.org/10.1093/hmg/ddw363.
[59] E. Tanaka, T. Ho, M.W. Kirschner, The role of microtubule dynamics in growth cone motility and axonal growth, J. Cell Biol. 128 (1995) 139–155.
[60] H. Witte, D. Neukirchen, F. Bradke, Microtubule stabilization specifies initial neuronal polarization, J. Cell Biol. 180 (2008) 619–632, https://doi.org/10.1083/jcb.200707042.

[61] M. Shvedunova, A. Akhtar, Modulation of cellular processes by histone and non-histone protein acetylation, Nat. Rev. Mol. Cell Biol. 23 (2022) 329–349, https://doi.org/10.1038/s41580-021-00441-y.
[62] M. He, Y. Ding, C. Chu, J. Tang, Q. Xiao, Z.-G. Luo, Autophagy induction stabilizes microtubules and promotes axon regeneration after spinal cord injury, Proc. Natl. Acad. Sci. U.S.A. 113 (2016) 11324–11329.
[63] M.A. Anderson, T.M. O'Shea, J.E. Burda, Y. Ao, S.L. Barlatey, A.M. Bernstein, J. H. Kim, N.D. James, A. Rogers, B. Kato, A.L. Wollenberg, R. Kawaguchi, G. Coppola, C. Wang, T.J. Deming, Z. He, G. Courtine, M.V. Sofroniew, Required growth facilitators propel axon regeneration across complete spinal cord injury, Nature 561 (2018) 396–400, https://doi.org/10.1038/s41586-018-0467-6.
[64] L.M. Milich, C.B. Ryan, J.K. Lee, The origin, fate, and contribution of macrophages to spinal cord injury pathology, Acta Neuropathol. 137 (2019) 785–797, https://doi.org/10.1007/s00401-019-01992-3.
[65] A. Akbari, N. Jabbari, R. Sharifi, M. Ahmadi, A. Vahhabi, S.J. Seyedzadeh, M. Nawaz, S. Szafert, M. Mahmoodi, E. Jabbari, R. Asghari, J. Rezaie, Free and hydrogel encapsulated exosome-based therapies in regenerative medicine, Life Sci. 249 (2020), 117447, https://doi.org/10.1016/j.lfs.2020.117447.
[66] M. Yao, J. Li, J. Zhang, S. Ma, L. Wang, F. Gao, F. Guan, Dual-enzymatically cross-linked gelatin hydrogel enhances neural differentiation of human umbilical cord mesenchymal stem cells and functional recovery in experimental murine spinal cord injury, J. Mater. Chem. B 9 (2021) 440–452, https://doi.org/10.1039/d0tb02033h.
[67] Y. Qian, J. Gong, K. Lu, Y. Hong, Z. Zhu, J. Zhang, Y. Zou, F. Zhou, C. Zhang, S. Zhou, T. Gu, M. Sun, S. Wang, J. He, Y. Li, J. Lin, Y. Yuan, H. Ouyang, M. Yu, H. Wang, DLP printed hDPSC-loaded GelMA microsphere regenerates dental pulp and repairs spinal cord, Biomaterials 299 (2023), 122137, https://doi.org/10.1016/j.biomaterials.2023.122137.